Cellular/Molecular

Differences between Dorsal Root and Trigeminal Ganglion Nociceptors in Mice Revealed by Translational Profiling

Salim Megat,[1,2] Pradipta R. Ray,[1,2] Diana Tavares-Ferreira,[1] Jamie K. Moy,[1] Ishwarya Sankaranarayanan,[1,2] Andi Wanghzou,[1,2] Tzu Fang Lou,[3] Paulino Barragan-Iglesias,[1,2] Zachary T. Campbell,[2,3] Gregory Dussor,[1,2] and Theodore J. Price[1,2]

[1]School of Behavioral and Brain Sciences, [2]Center for Advanced Pain Studies, and [3]Department of Biological Sciences, University of Texas at Dallas, Richardson, Texas, 75080

Nociceptors located in the trigeminal ganglion (TG) and DRG are the primary sensors of damaging or potentially damaging stimuli for the head and body, respectively, and are key drivers of chronic pain states. While nociceptors in these two tissues show a high degree of functional similarity, there are important differences in their development lineages, their functional connections to the CNS, and recent genome-wide analyses of gene expression suggest that they possess some unique genomic signatures. Here, we used translating ribosome affinity purification to comprehensively characterize and compare mRNA translation in *Scn10a*-positive nociceptors in the TG and DRG of male and female mice. This unbiased method independently confirms several findings of differences between TG and DRG nociceptors described in the literature but also suggests preferential utilization of key signaling pathways. Most prominently, we provide evidence that translational efficiency in mechanistic target of rapamycin (mTOR)-related genes is higher in the TG compared with DRG, whereas several genes associated with the negative regulator of mTOR, AMP-activated protein kinase, have higher translational efficiency in DRG nociceptors. Using capsaicin as a sensitizing stimulus, we show that behavioral responses are greater in the TG region and this effect is completely reversible with mTOR inhibition. These findings have implications for the relative capacity of these nociceptors to be sensitized upon injury. Together, our data provide a comprehensive, comparative view of transcriptome and translatome activity in TG and DRG nociceptors that enhances our understanding of nociceptor biology.

Key words: DRG; mTOR; neuropathic pain; TG; TRAP

Significance Statement

The DRG and trigeminal ganglion (TG) provide sensory information from the body and head, respectively. Nociceptors in these tissues are critical first neurons in the pain pathway. Injury to peripheral neurons in these tissues can cause chronic pain. Interestingly, clinical and preclinical findings support the conclusion that injury to TG neurons is more likely to cause chronic pain and chronic pain in the TG area is more intense and more difficult to treat. We used translating ribosome affinity purification technology to gain new insight into potential differences in the translatomes of DRG and TG neurons. Our findings demonstrate previously unrecognized differences between TG and DRG nociceptors that provide new insight into how injury may differentially drive plasticity states in nociceptors in these two tissues.

Introduction

Mechanical, thermal, and chemical peripheral stimuli are detected by the pseudo-unipolar sensory neurons of the DRG and the trigeminal ganglion (TG) (Devor, 1999; Woolf and Ma, 2007; Dubin and Patapoutian, 2010). Neurons in the DRG transmit signals from the limbs and body, including much of the viscera, to the CNS through the dorsal horn of the spinal cord. TG neurons relay sensory information from the head and face through a region of the dorsal brainstem known as the trigeminal nucleus caudalis. Although TG and DRG neurons express similar markers and are often considered as very similar, there are differences in

Received Oct. 15, 2018; revised June 19, 2019; accepted June 20, 2019.

Author contributions: S.M., P.R.R., Z.T.C., G.D., and T.J.P. designed research; S.M., P.R.R., D.T.-F., J.K.M., I.S., A.W., T.F.L., P.B.-I., and T.J.P. performed research; S.M., P.R.R., and D.T.-F. analyzed data; S.M., P.R.R., A.W., Z.T.C., G.D., and T.J.P. edited the paper; S.M., P.R.R., G.D., and T.J.P. wrote the paper; T.J.P. wrote the first draft of the paper.

This work was supported by National Institutes of Health Grant R01NS065926 to T.J.P., Grant R01NS098826 to T.J.P. and G.D., and Grant R01NS100788 to Z.T.C., University of Texas STARS program to T.J.P. and G.D., and a postdoctoral CONACYT fellowship program to P.B.-I. Raw RNA sequencing data are available through GEO: GSE 113941. Transgenic mice are available through The Jackson Laboratory. All raw data and code are available upon request.

The authors declare no competing financial interests.

Correspondence should be addressed to Theodore J. Price at Theodore.price@utdallas.edu.

https://doi.org/10.1523/JNEUROSCI.2663-18.2019

their cellular populations (Price and Flores, 2007). The tissues also have distinct embryonic origins with important functional consequences (Durham and Garrett, 2010). Finally, neurons in these ganglia innervate distinct targets in the periphery (e.g., the teeth and dura mater for the TG) and in the CNS. An excellent example of this differential innervation in the CNS is the discovery of a subset of TG nociceptors that bypass the traditional second-order relay in the nucleus caudalis projecting directly to the parabrachial nucleus (Rodriguez et al., 2017). These findings suggest distinct molecular signatures of DRG and TG neurons that may be important for understanding sensory neurobiology from these different regions of an organism.

Advances in next-generation sequencing have allowed the characterization of DRG and TG tissues at the genome-wide level using RNA sequencing (RNA-seq) (Manteniotis et al., 2013; Reynders et al., 2015; Gong et al., 2016; Hu et al., 2016; Kogelman et al., 2017). These studies provide significant insight into genes that are differentially expressed between these tissues, including differences between species (Manteniotis et al., 2013; Flegel et al., 2015; Kogelman et al., 2017). However, these studies lack cell-type specificity and fail to capture translational efficiency. Cell specificity is a key advantage for single-cell transcriptomic methods (Usoskin et al., 2015; Hu et al., 2016) and other cellular enrichment protocols (Isensee et al., 2014; Thakur et al., 2014; Lopes et al., 2017) that have now been applied to the DRG and/or TG. However, only one direct comparison has thus far been made between TG and DRG transcriptomes using neuronal enrichment followed by RNA-seq (Lopes et al., 2017). Examining ribosome-bound RNA is advantageous because there is strong evidence that transcriptional and translational efficiencies are decoupled in most cells (Fortelny et al., 2017). Methods that sequence ribosome-bound RNAs give more accurate predictions of cellular proteomes (Heiman et al., 2008; Ingolia, 2016). Two techniques have emerged in this area. The first, ribosome footprint profiling, comprehensively and quantitatively provides a snapshot of translation activity at single codon resolution through deep sequencing of ribosome-protected mRNA fragments from cells or tissues (Ingolia, 2016). This technique, which has recently been applied to the DRG (Uttam et al., 2018), does not allow insight into cell-type-specific translational profiling. A second technique is translating ribosome affinity purification (TRAP), which relies on genetic tagging of ribosomal proteins for cell-specific pulldown of translating ribosomes bound to mRNAs for RNA-seq (Doyle et al., 2008; Heiman et al., 2008, 2014). This technique lacks the single codon resolution of ribosome footprint profiling but allows for precise assessment of cellular translatomes *in vitro* and *in vivo*.

Here we used the TRAP technology using the Nav1.8^{Cre} mouse (Stirling et al., 2005) to achieve sensory neuron-specific ribosome tagging with enrichment in the nociceptor population. We then compared TG and DRG nociceptor translatomes and quantified mRNAs that are differentially expressed at the transcriptional and/or translational level. Interestingly, we found that translational activity of mechanistic target of rapamycin (mTOR)-related genes is higher in the TG compared with DRG. Given the key role that this signaling pathway plays in rapid sensitization of nociceptors (Khoutorsky and Price, 2018), this result is intriguing because activation of nociceptors in the facial region produces greater sensitization and perceived pain in human subjects (Schmidt et al., 2015, 2016), an effect that our experiments also demonstrate in mice. Therefore, our work pinpoints important signaling differences between DRG and TG nociceptors that have direct functional consequences on the susceptibility of these nociceptors to rapid sensitization.

Materials and Methods

Transgenic animals: Nav1.8^{cre}/Rosa26^{fsTRAP} mice. All animal procedures were approved by the Institutional Animal Care and Use Committee of University of Texas at Dallas.

Rosa26^{fsTRAP} mice were purchased from The Jackson Laboratory (stock #022367). Transgenic mice expressing Cre recombinase under the control of the Scn10a (Nav1.8) promoter were obtained initially from Professor John Wood (University College London) but are commercially available from Infrafrontier (EMMA ID: 04582). The initial characterization of these mice demonstrated that the introduction of the Cre recombinase in heterozygous animals does not affect pain behavior, and their DRG neurons have normal electrophysiological properties (Stirling et al., 2005). Nav1.8^{cre} mice on a C57BL/6J genetic background were maintained and bred at the University of Texas at Dallas. Upon arrival, Rosa26^{fsTRAP} mice were crossed to *Nav1.8^{cre}* to generate the Nav1.8-TRAP mice that express a fused EGFP-L10a protein in Nav1.8-expressing neurons. All experiments were performed using male and female littermates 8–12 weeks old. Mice were group housed (4 maximum) in non-environmentally enriched cages with food and water *ad libitum* on a 12 h light-dark cycle. Room temperature was maintained at 21 ± 2°C.

TRAP. Nav1.8-TRAP male and female mice were decapitated and DRG and TG rapidly dissected in ice-cold dissection buffer (1× HBSS; Invitrogen, 14065006), 2.5 mM HEPES, 35 mM glucose, 4 mM $NaHCO_3$, 100 μg/ml cycloheximide, 0.001V 2 mg/ml emetine). DRGs or TGs were transferred to ice-cold polysome buffer (20 mM HEPES, 12 mM $MgCl_2$, 150 mM KCl, 0.5 mM DTT, 100 μg/ml cycloheximide, 20 μg/ml emetine, 40 U/ml SUPERase IN, Promega, 1 μl DNase, and protease inhibitor) and homogenized using a Dounce homogenizer. Samples were centrifuged at 3000 × *g* for 10 min to prepare postnuclear fraction (S1). Then, 1% NP-40 and 30 mM 1,2-dihexanoyl-sn-glycero-3-phosphocholine were added to the S1 fraction and then centrifuged at 15,000 × *g* for 15 min to generate a postmitochondrial fraction (S20). A 200 μl sample of S20 was removed for use as Input, and 800 μl of S20 was incubated with protein G-coated Dynabeads (Invitrogen) bound to 50 μg of anti-GFP antibodies (HtzGFP-19F7 and HtzGFP-19C8, Memorial Sloan Kettering Centre) for 3 h at 4°C with end-over-end mixing. Anti-GFP beads were washed with high salt buffer (20 mM HEPES, 5 mM $MgCl_2$, 350 mM KCl, 1% NP-40, 0.5 mM DTT, and 100 μg/ml cycloheximide), and RNA was eluted from all samples using a Direct-zol kit (Zymo Research) according to the manufacturer's instructions. RNA yield was quantified using a Nanodrop system (Thermo Fisher Scientific), and RNA quality was determined by fragment analyzer (Advanced Analytical Technologies).

Library generation and sequencing. Libraries were generated from 100 ng to 1 μg of total RNA using Quantseq 3′ mRNA-Seq library kit (Lexogen) with RiboCop rRNA depletion kit (Lexogen) treatment according to the manufacturer's protocols. The endpoint PCR amplification cycle number for each sample was determined by qPCR assay with PCR Add-on kit for Illumina (Lexogen). The cycle number was selected when the fluorescence value reached 33% of the maximum for each sample. Purified libraries were quantified by Qubit (Invitrogen), and the average size was determined by fragment analyzer (Advanced Analytical Technologies) with high-sensitivity next-generation sequencing fragment analysis kit. Libraries were then sequenced on an Illumina NextSeq500 Sequencer using 50 bp single-end reads.

Sequence files generated by the Illumina NextSeq500 Sequencer were downloaded from BaseSpace. An initial quality check using FastQC 0.11.5 (Babraham Bioinformatics) was done on the sequencing files, and then trimming was performed on the server with the FASTQ Toolkit. Sequences were trimmed with optimized parameters (13 bases from 3′ end, 17 bases from 5′ end, and any poly-adenine longer than 2 bases from the 3′ side). Trimming parameters were optimized based on FastQC results and mapping rate, as well as manually checking high reads or abundant chromosomal regions with IGV 2.3.80. The trimmed sequencing samples were then processed using TopHat 2.1.1 (with Bowtie 2.2.9) and mapped to the mouse reference genome (NCBI reference assembly GRCm38.p4) and reference transcriptome (Gencode vM10) generating

files in .bam format. Processed .bam files were then quantified for each gene using Cufflinks 2.2.1 with gencode.vM10 genome annotation. Because reads only mapped to the 3′UTR of the gene, read counts were not normalized by length by using the Cufflinks option − no-length-correction. Relative abundance for the ith gene was determined by calculating TPM (transcripts per million) values as follows:

$$TPM_i = 10^6 \times \frac{a_i}{\sum_j [a_j]}$$

where a_j is the Cufflinks reported relative abundance. Finally, TPM values were normalized to upper decile for each biological replicate, and udTPM (upper decile TPM) were used for analysis (Glusman et al., 2013). This was done to provide uniform processing for samples with varying sequencing depth and because of varying number of genes in the transcriptome and translatome samples.

Behavioral procedures. Female C57BL/6J mice were injected subdermally with capsaicin (0.1 μM) into either cheek or hindpaw in a volume of 10 μl with Hamilton syringe and 30G needle. For cheek injections, mice cheeks were shaved 3 d before injections. AZD8055 (mTORC1 inhibitor) or vehicle was administered intraperitoneally (10 mg/kg) 2 h before capsaicin injections into the cheek. AZD8055 was dissolved in DMSO (50 mg/ml) and further diluted in 30% (w/v) cyclodextrin to make up the correct dose for each animal. Vehicle consisted of 10% DMSO and 30% w/v cyclodextrin. Baseline videos were recorded for 15 min for each mouse. After cheek or hindpaw injections, experimental videos were recorded for 60 min. The recording setup consisted of one camera in front and one in the back. The sum of facially directed behaviors with the forepaws following injection of capsaicin into the whisker pad as well as the number of hindpaw directed behaviors for the hindpaw were scored and classified as nocifensive behaviors.

The Mouse Grimace Scale was used to quantify affective aspects of pain in mice (Langford et al., 2010). We scored the changes in the facial expressions (using the facial action coding system) at baseline and then 15 and 30 min after intraplantar or facial injection of capsaicin.

qRT-PCR. Lumbar DRGs and TGs were isolated from 4 male mice per genotype and flash-frozen on dry ice and stored at −80°C until ready to be processed. Tissues were homogenized using a pestle, and total RNA was extracted using RNAqueous Total RNA Isolation kits (Thermo Fisher Scientific). RNA was subsequently treated with TURBO DNase (Thermo Fisher Scientific) according to the manufacturer's instructions. RNA concentration was measured on a NanoDrop 2000 (Thermo Fisher Scientific). cDNA was synthesized using iScript Reverse Transcriptase (Bio-Rad). qRT-PCR was done using a Applied Biosystems Lightcycler 7500 Real-Time PCR system using iTaq Universal SYBR Green Supermix (Bio-Rad) according to the manufacturer's instructions with 3 technical replicates per biological replicate (averages of the technical replicates per biological replicate are reported) using primers pairs: *Gapdh* forward 5′-GACAACTTTGGCATTGTGGA-3′ and *Gapdh* reverse 5′-CATCA TACTTGGCAGGTTTCTC-3′, *Rraga* forward 5′-ACGTCCGATTCT TGGGGAAC-3′ and *Rraga* reverse 5′-TACGGAAGATGTTGTCCCGC-3′, *Fth* forward 5′-GCACTGCACTTGGAAAAGAGT-3′ and *Fth* reverse 5′-ACGTGGTCACCCAGTTCTTT-3′. Primers were made by Integrated DNA Technologies.

Primer efficiency curves were determined by diluting total RNA of DRG and TG samples with 6 points of 1:5 serial dilutions. RNA dilutions were then converted to cDNA, and standard curves were determined for DRG and TG with each primer set separately. Concentrations resulting in multiple products or incorrect product size via melt-curve analysis (derivative reporter vs temperature) were omitted. Efficiencies for each primer set for DRGs and TGs were calculated using the Applied Biosystems 7500 software version 2.3. Total RNA (115 ng) used in experiments fell within primer standard curves with efficiencies between 85% and 110%. Data were analyzed as $2^{-\Delta\Delta Ct}$ and normalized as shown in Results.

Antibodies. The peripherin antibody used for immunohistochemistry were obtained from Sigma-Aldrich. Isolectin B_4 (IB_4) conjugated to AlexaFluor-568 and secondary AlexaFluor antibodies were purchased from Invitrogen. Calcitonin gene-related peptide (CGRP) antibody was purchased from Peninsula Laboratories. RagA and Akt1s1 (also known as PRAS40) antibodies were from Cell Signaling Technology. Antibodies for TRAP (HtzGFP-19F7 and HtzGFP-19C8) were obtained from Sloan Memorial Kettering Centre, after establishing Material Transfer Agreements with the laboratory of Prof. Nathaniel Heintz (Rockefeller University).

Immunohistochemistry. Animals were anesthetized with isoflurane (4%) and killed by decapitation, and tissues were flash-frozen in OCT on dry ice. Sections of TG (20 μm) were mounted onto SuperFrost Plus slides (Thermo Fisher Scientific) and fixed in ice-cold 10% formalin in 1× PBS for 45 min, and then subsequently washed 3 times for 5 min each in 1× PBS. Slides were then transferred to a solution for permeabilization made of 1× PBS with 0.2% Triton X-100 (Sigma-Aldrich). After 30 min, slides were washed 3 times for 5 min each in 1× PBS. Tissues were blocked for at least 2 h in 1× PBS and 10% heat-inactivated normal goat serum. TG or DRG slices were stained with peripherin, CGRP, and IB_4 conjugated to AlexaFluor-568. Immunoreactivity was visualized following 1 h incubation with goat anti-rabbit, goat anti-mouse, and goat anti-guinea pig AlexaFluor antibodies at room temperature. All immunohistochemical images are representations of samples taken from 3 animals per genotype. Images were taken using an Olympus FluoView 1200 confocal microscope. Analysis of images was done using ImageJ Version 1.48 for Apple OSX (National Institutes of Health).

Western blotting. Male and female mice were used for all Western blotting experiments and were killed by decapitation while under anesthesia and tissues (DRG or TG) were flash frozen on dry ice. Frozen tissues were homogenized in lysis buffer (50 mM Tris, pH 7.4, 150 mM NaCl, 1 mM EDTA, pH 8.0, and 1% Triton X-100) containing protease and phosphatase inhibitors (Sigma-Aldrich), and homogenized using a pestle. A total of 15 μg of protein was boiled for 5 min in loading dye and then loaded into each well and separated by a 10%–12% SDS-PAGE gel. Proteins were transferred to a 0.45 μm PVDF membrane (Millipore) at 25 V overnight at 4°C. Subsequently, membranes were blocked with 5% nonfat dry milk in 1× Tris buffer solution containing Tween 20 (TTBS) for 3 h. Membranes were washed in 1× TTBS 3 times for 5 min each, then incubated with primary antibody overnight at 4°C. The following day, membranes were washed 3 times in 1× TTBS for 5 min each, then incubated with the corresponding secondary antibody at room temperature for 1 h. Membranes were then washed with 1× TTBS 5 times for 5 min each. Signals were detected using Immobilon Western Chemiluminescent HRP substrate (Millipore). Bands were visualized using film (Kodak) or with a Bio-Rad ChemiDoc Touch. Membranes were stripped using Restore Western Blot Stripping buffer (Thermo Fisher Scientific) and reprobed with another antibody. Analysis was performed using Image Lab (Bio-Rad).

Statistics. All data are presented as mean ± SEM. All analysis was done using GraphPad Prism 6 version 6.0 for Mac OS X. Single comparisons were performed using Student's *t* test or one-way ANOVA if multiple groups were compared. For behavioral experiments, two-way ANOVA (time × treatment) was used to measure effects across time between different groups. If significant effects were found by ANOVA, *post hoc* analyses were performed. Multiple comparisons between groups/within groups were performed using Sidak's correction. Statistical results can be found in the figure legends.

Statistics for RNA sequencing. Differential expression analysis was performed using MATLAB scripts. TPM values were normalized to their 90th percentile to generate udTPMs, and the probability density function of the udTPM was used to set the threshold value for further analysis. Genes showing consistent expression above the set threshold across biological replicates were then used to generate lists of differentially expressed genes. Standard *t* test was first performed assuming unequal variances between experimental groups generating *p* values for each gene as follows. A *q* value for the ith test was then calculated using Benjamini–Hochberg correction for multiple comparisons as follows:

$$Qvalue_i = \frac{pvalue_i \times N}{rank_{pualue_i}}$$

where *N* is the number of tests.

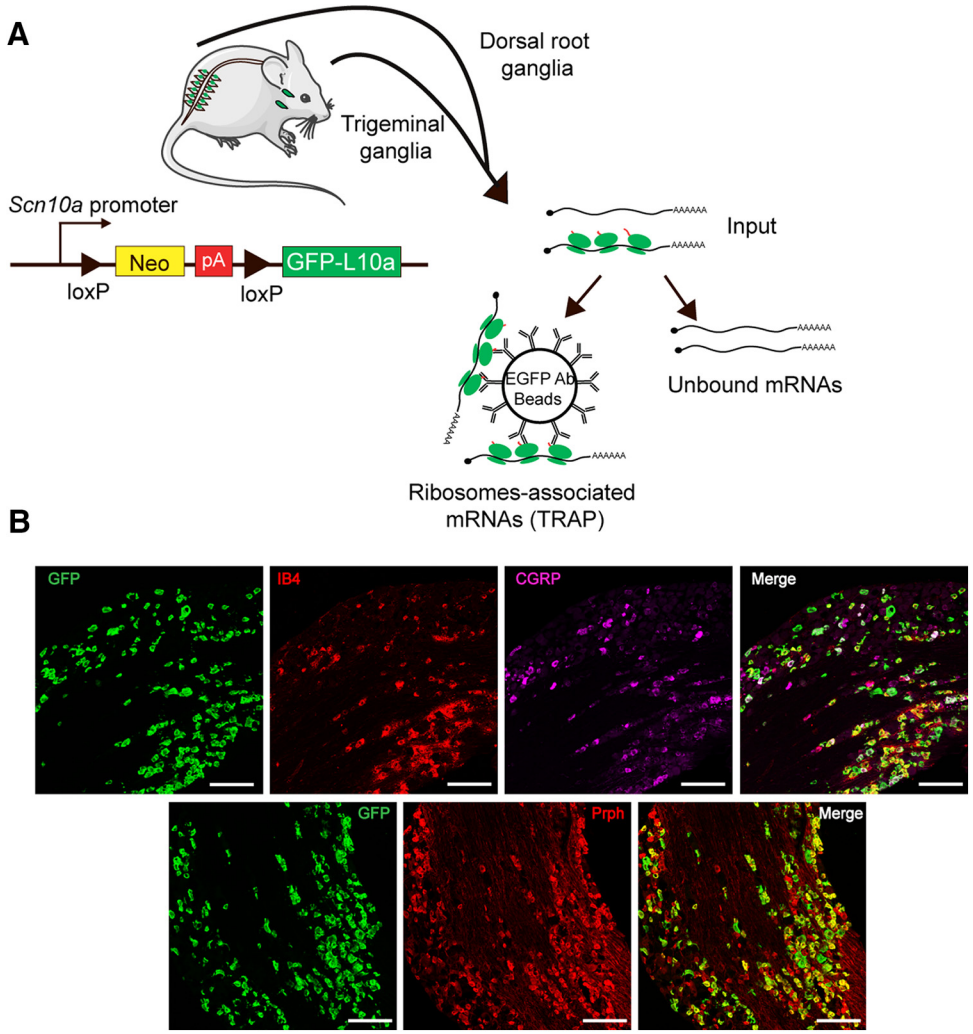

Figure 1. TRAP-seq strategy and expression in TG. ***A***, Schematic representation of TRAP-seq approach showing isolation of translating ribosomes with immunoprecipitation using anti-GFP-coated beads. ***B***, Immunostaining of CGRP, IB_4, and peripherin (Prph) on TG sections from Nav1.8-TRAP mice (GFP). Scale bar, 100 μm.

Finally, the cumulative density function of the fold change was plotted and used to set the fold change for the input and TRAP fraction for both DRG and TG datasets. Gene set enrichment analyses were performed with Enrichr (Kuleshov et al., 2016) using the Gene Ontology molecular function 2015 term, the biological process 2015 term, and the Reactome 2015 libraries.

For motif finding, 5′-UTR sequences of corresponding genes were obtained from gencode.vM10 (mouse genome assembly GRCm38), with all transcript isoforms kept for analysis. As most 5′-UTRs of different isoforms from the same gene share partial/whole sequences with each other, when a 5′-UTR sequence was fully shared by another longer 5′-UTR isoform of the same gene, the shorter version was removed to prevent genes with a large amount of isoforms being overrepresented in the motif analysis. All 5′-UTR sequences remaining after filtering were then passed through MEME Suite 5.0.2 for motif discovery, with the following parameters: all motifs are within 10–20 bp length range, only found on the provided strand, and appear in at least 10% of the genes provided. Motifs appearing in >30% of the genes with significant *E* value are shown in the text.

Results

To generate nociceptor-TRAP mice, $Nav1.8^{cre}$ animals were crossed with $Rosa26^{fs\text{-}TRAP}$ (Zhou et al., 2013) to express the eGFP fused to the ribosomal L10a protein in $Nav1.8^{+}$ neurons. This approach generates Nav1.8-TRAP neurons in both the DRG and TG. While the specificity of our approach was recently shown in the DRG (Megat et al., 2019), we characterized expression of the transgene in the TG (Fig. 1*A*). We found that eGFP-L10a-positive neurons primarily colocalized with small-diameter peripherin-positive neurons and that extensive overlap was found with both CGRP immunoreactivity and with IB_4 staining (Fig. 1*B*). These findings demonstrate that this technique labels an equivalent subset of neurons in the DRG and TG of mice.

Having confirmed that the Nav1.8-TRAP approach yields robust expression in nociceptors in the TG, we set out to conduct TRAP sequencing to compare nociceptor translatomes in the DRG and TG. To successfully isolate ribosome-associated mRNAs from Nav1.8-TRAP cells, we determined that TGs from 4 animals were required for a single biological replicate. This number matches the number of DRGs needed for TRAP sequencing. To make comparisons between the TG and DRG, we generated TRAP sequencing from the TG that was then compared with our previously generated DRG dataset (GSE 113941). We sequenced the total mRNA input from all biological replicates and mRNAs associated with translating ribosomes in the Nav1.8 subset of TG neurons, equivalently to what was done from DRG (Megat et al., 2019). This approach allowed us to make comparisons between

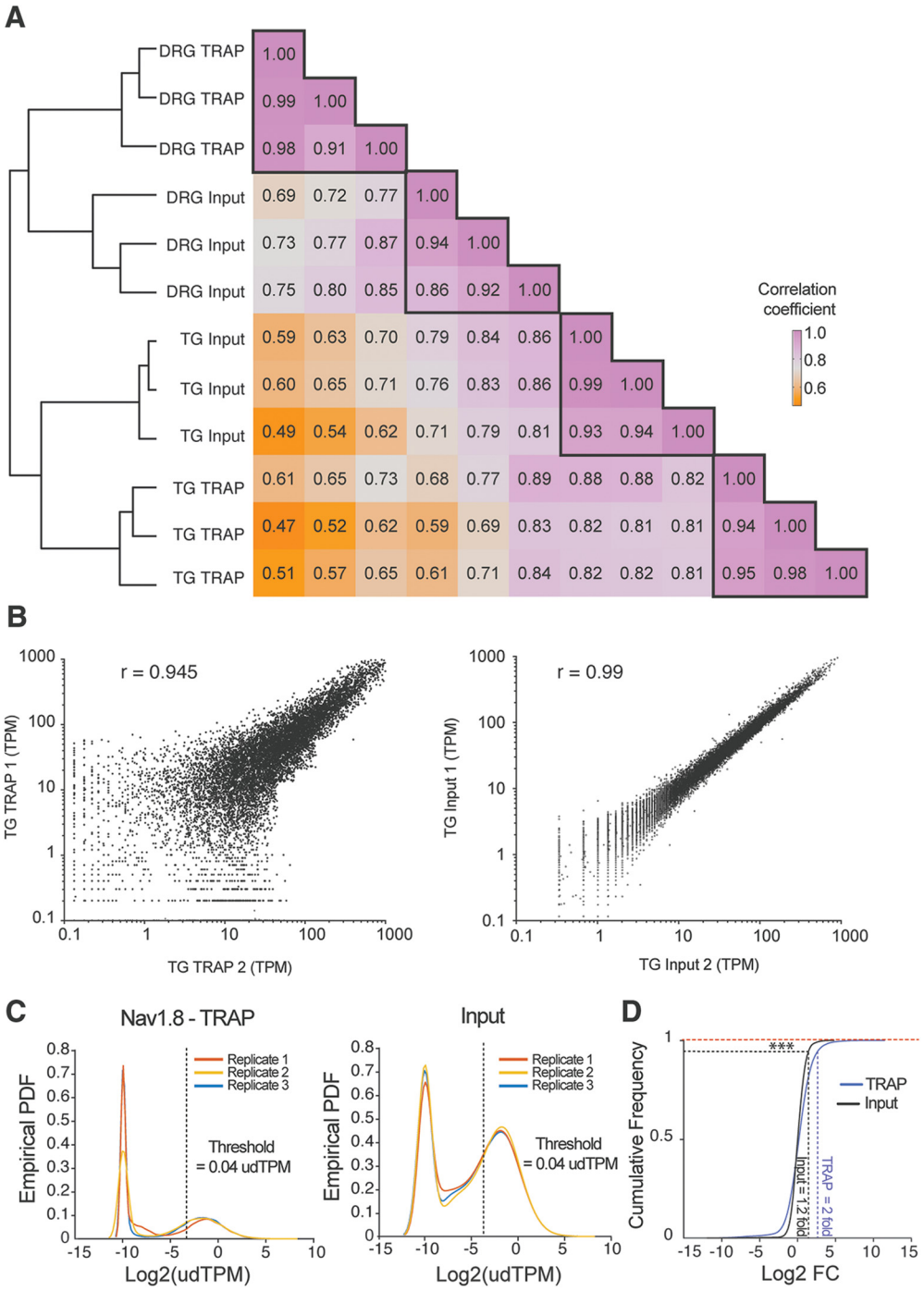

Figure 2. DRG and TG TRAP-seq shows high correlation between biological replicates and similar sequencing depth. ***A***, Heatmap of the correlation coefficient and cluster analysis showing clear separation between DRG and TG as well as in between TRAP-seq and bulk RNA-seq from each tissue. ***B***, Scatter plot of input and TRAP-seq shows high correlation between biological replicates for each approach. ***C***, Empirical probability density function (PDF) of the TPM for all genes in analysis shows a similar distribution between replicates, which are each shown as a different color, for TRAP-seq and input. ***D***, Cumulative distribution of the fold change (FC) in input and TRAP-seq shows higher FCs in TRAP-seq samples. Kolgomorov-Smirnov test, $^{***}p < 0.001$.

the whole tissue transcriptional and Nav1.8$^+$ neuron translational landscapes between DRG and TG.

The first dimension of the clustering analysis identified clear differences between TG and DRG as well as distinctions within each subcluster comprised of the input (transcriptome) and TRAP (translatome) RNA sequencing (Fig. 2*A*). We observed strong correlation coefficients between biological replicates demonstrating low variability in the experimental protocol (Fig. 2*B*). Gene expression values (TPMs) were normalized to the 90th percentile for each biological replicate, and the empirical probability density function of the normalized expression level (upper decile (ud)TPM) was plotted for the input and TRAP fractions (Fig. 2*C*). The probability density function identified 2 peaks, and the inflection point was used to set the threshold expression values according to the sequencing depth (Fig. 2*C*). After further filtering, based on consistent expression among biological replicates, we included a total of 7358 genes in the final analysis to make comparisons between the DRG and TG transcriptomes and

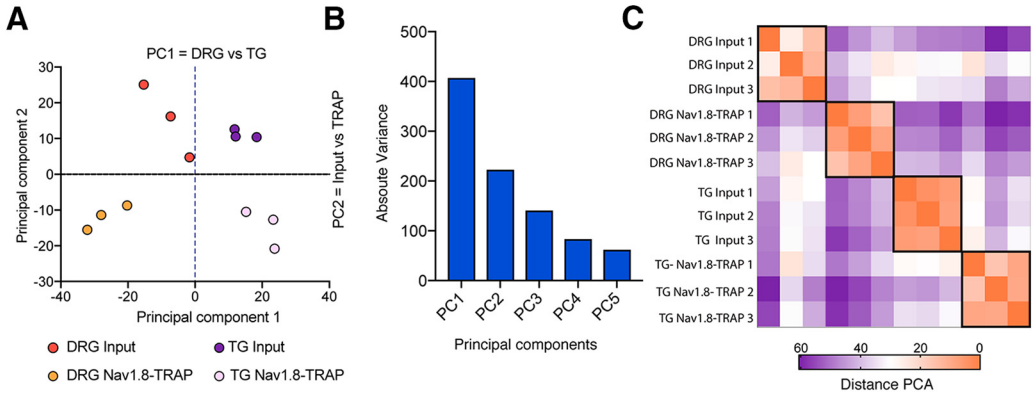

Figure 3. PC analysis shows a clear difference between transcriptomes and translatomes in TG and DRG. ***A***, PC analysis shows that differences between TG and DRGs whole tissue transcriptomes represent the first PC, whereas differences between transcriptome and translatome are the second PC. ***B***, Absolute variances for each PC show that PC1 and PC2 provide the majority of variation in the entire datasets. ***C***, Heatmap of the absolute PC distances showing 4 distinct clusters, each of which is defined by whole transcriptome (input) versus TRAP-seq and the tissue.

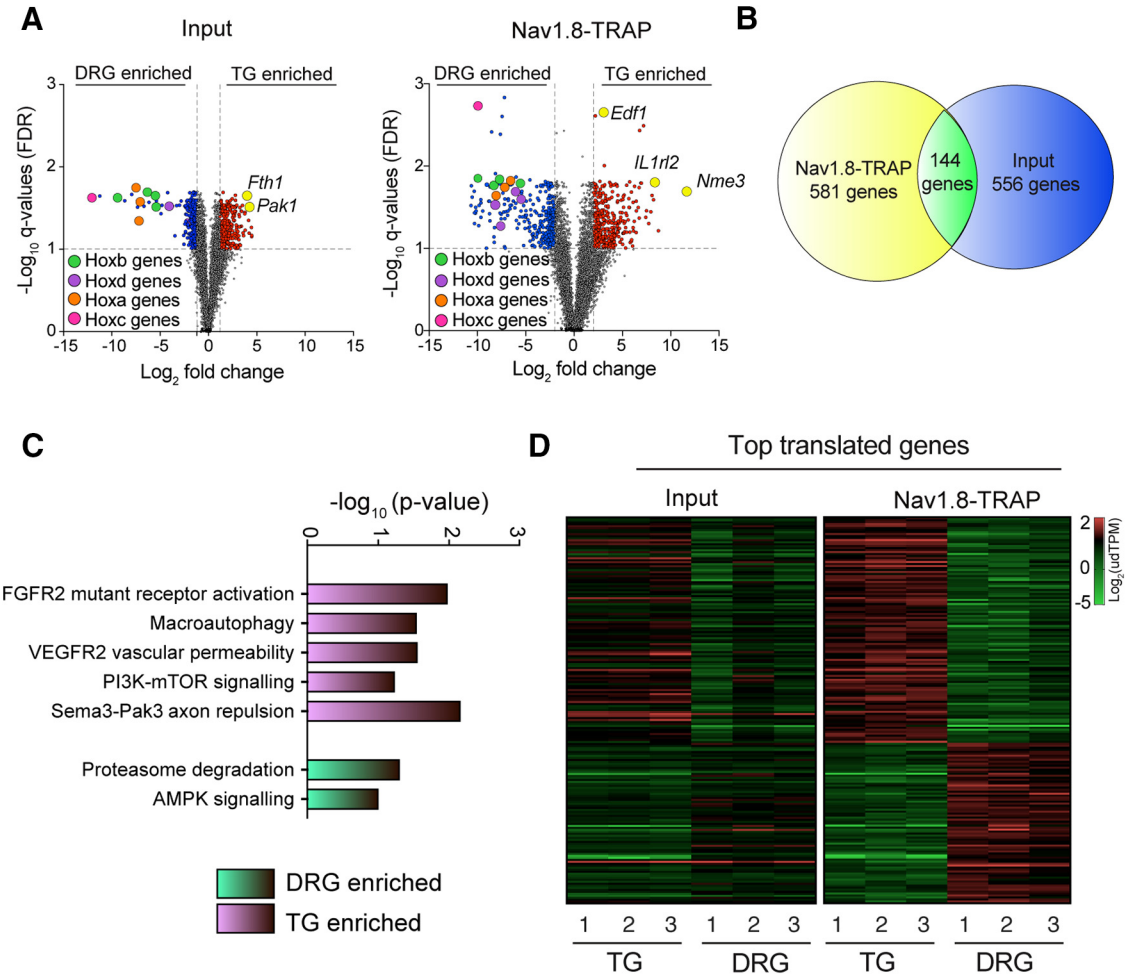

Figure 4. Transcriptomic and translatomic differences between the TG and DRG of mice. ***A***, ***B***, Volcano plots showing genes that are enriched in the DRG or TG in the whole tissue transcriptome (input) or in the TRAP-seq sample (Nav1.8-TRAP) with genes highlighted in the text labeled (yellow dots). ***C***, GO term analysis of the TRAP-seq-enriched mRNAs in DRG or TG using EnrichR (adjusted p value < 0.05) shows an enrichment in AMPK-related genes in the DRGs, whereas mTOR-related genes are highly translated in the TG. ***D***, Heatmaps showing the expression level of enriched mRNAs (input) and enriched translated mRNAs (Nav1.8 TRAP) in both tissues showing discordance between the transcriptome and translatome mRNA levels.

Nav1.8-TRAP translatomes. Finally, we plotted the cumulative frequency distribution as a function of the log twofold change for each of these 7358 genes in TG and DRG biological replicates, and the 95th percentile was used to set the threshold fold change values for the input and TRAP fractions (Fig. 2*D*). Principal component (PC) analysis indicated that PC1 distinguished between TG and DRG, whereas PC2 detected a difference between input and Nav1.8-TRAP, suggesting a clear transcriptional and translational signature for both of these tissues (Fig. 3*A*). Detailed analysis of the variances for each PC clearly showed that the first

Table 1. Genes upregulated in the TG input

Genes	Log2 fold change	*p*	*q*	Genes	Log2 fold change	*p*	*q*
1700037C18Rik	1.847	0.006	0.058	*Mrpl36*	1.645	0.024	0.100
6430548M08Rik	1.249	0.000	0.026	*Mrpl44*	1.331	0.020	0.093
9130401M01Rik	1.884	0.023	0.098	*Mrpl46*	1.476	0.005	0.052
Aard	2.059	0.001	0.030	*Mrps11*	1.718	0.003	0.042
Abca2	1.917	0.000	0.026	*Mrps14*	1.614	0.004	0.050
Abhd6	1.493	0.001	0.031	*Mrps23*	1.332	0.001	0.031
Adarb1	1.426	0.011	0.072	*Mrps36*	1.262	0.002	0.034
Adck2	1.969	0.004	0.049	*Mt2*	3.017	0.023	0.097
Ak5	1.564	0.004	0.050	*Mt3*	2.988	0.011	0.071
Alkbh3	2.585	0.002	0.039	*Mtap*	1.600	0.017	0.086
Amdhd2	1.234	0.001	0.030	*Mtfp1*	1.528	0.001	0.034
Anapc13	1.952	0.003	0.046	*Mtmr4*	1.402	0.005	0.052
Ap4s1	1.506	0.006	0.057	*Mxd3*	1.297	0.020	0.092
Apbb1	3.191	0.005	0.054	*Mxra8*	2.100	0.004	0.051
Apip	1.677	0.023	0.099	*Myl12a*	2.141	0.000	0.027
Apmap	1.356	0.007	0.061	*Mylk*	1.285	0.019	0.090
Apod	3.523	0.001	0.029	*Naa38*	3.315	0.019	0.090
Apoe	1.621	0.018	0.088	*Nap1l2*	1.759	0.002	0.035
Arfip2	1.328	0.000	0.026	*Ndp*	1.418	0.005	0.053
Arhgef3	1.405	0.014	0.079	*Ndufa12*	1.436	0.012	0.073
Arhgef4	1.255	0.005	0.055	*Ndufa13*	1.921	0.024	0.100
Arih2	1.638	0.008	0.066	*Ndufb2*	3.404	0.005	0.053
Armc5	1.203	0.020	0.093	*Necab3*	1.663	0.007	0.062
Arpc5l	1.248	0.021	0.095	*Nefh*	1.820	0.001	0.031
Atp5c1	2.858	0.012	0.074	*Nif3l1*	1.999	0.018	0.087
Atp5d	2.923	0.004	0.052	*Nme3*	3.589	0.008	0.063
Atp5j	2.373	0.011	0.070	*Nnat*	1.368	0.023	0.099
Atp5sl	1.335	0.005	0.053	*Nr2f6*	1.334	0.016	0.084
Atxn7l3	1.365	0.015	0.080	*Nsg1*	2.505	0.003	0.041
Avpi1	1.810	0.015	0.082	*Nsmaf*	1.511	0.002	0.037
B930041F14Rik	2.887	0.004	0.051	*Nubp2*	2.798	0.000	0.026
Bad	1.797	0.005	0.052	*Nudt1*	1.395	0.017	0.086
Bet1l	1.486	0.014	0.079	*Nudt13*	1.358	0.007	0.062
Bod1	1.529	0.013	0.077	*Odc1*	2.129	0.005	0.053
Cacng5	2.058	0.008	0.063	*Otud3*	2.021	0.002	0.037
Calb2	3.253	0.005	0.053	*P2rx6*	1.581	0.009	0.068
Calu	1.213	0.001	0.031	*Pacs2*	1.388	0.000	0.029
Camkk1	1.514	0.013	0.076	*Pak1*	3.982	0.001	0.030
Casp3	1.506	0.002	0.035	*Pard6a*	1.806	0.011	0.072
Cbx7	1.324	0.015	0.081	*Pced1a*	1.460	0.018	0.088
Ccdc12	1.344	0.018	0.087	*Pcp4l1*	1.512	0.000	0.020
Ccdc124	1.505	0.015	0.082	*Pdia4*	1.410	0.002	0.037
Ccdc63	3.251	0.018	0.088	*Pdlim2*	2.857	0.001	0.030
Cd81	1.413	0.005	0.055	*Pex11b*	2.281	0.017	0.086
Cda	1.665	0.003	0.044	*Pgbd5*	1.688	0.001	0.031
Cdc37	1.442	0.014	0.079	*Pin1*	1.948	0.013	0.076
Cdk5r1	1.482	0.005	0.055	*Pkdcc*	1.610	0.003	0.045
Cdpf1	1.216	0.014	0.079	*Pkm*	1.408	0.014	0.080
Cdr2l	1.629	0.015	0.082	*Pla2g16*	2.793	0.000	0.022
Cela1	1.982	0.014	0.080	*Plcd4*	1.204	0.015	0.082
Cenpf	3.061	0.020	0.091	*Plekha4*	1.487	0.001	0.030
Cep19	1.321	0.005	0.053	*Plk5*	2.167	0.007	0.063
Cgrrf1	2.813	0.002	0.035	*Pllp*	1.905	0.002	0.040
Chchd1	2.920	0.001	0.029	*Plpp1*	2.148	0.003	0.046
Chchd3	1.514	0.018	0.088	*Plxdc1*	1.659	0.003	0.046
Chga	1.707	0.007	0.063	*Pnpla2*	1.296	0.013	0.078
Chgb	1.656	0.002	0.039	*Polr2b*	1.215	0.021	0.095
Chmp6	2.654	0.003	0.045	*Polr2l*	4.483	0.010	0.070
Chpf2	1.312	0.015	0.082	*Pon2*	1.207	0.002	0.040
Chrac1	1.481	0.002	0.035	*Ppa2*	1.552	0.005	0.052
Ckmt1	1.257	0.020	0.093	*Ppdpf*	1.387	0.023	0.097
Clcn7	1.490	0.005	0.053	*Ppfia4*	2.311	0.001	0.030
Clec2l	2.448	0.002	0.036	*Ppm1f*	1.386	0.011	0.071
Clu	1.283	0.000	0.029	*Ppp1r16b*	1.798	0.023	0.097

(*Table continues*)

Table 1. Continued

Genes	Log2 fold change	*p*	*q*	Genes	Log2 fold change	*p*	*q*
Clybl	1.665	0.015	0.081	*Ppp2r4*	1.920	0.003	0.044
Cnnm4	1.420	0.022	0.097	*Prorsd1*	1.630	0.018	0.088
Cnp	2.467	0.000	0.024	*Prpsap1*	1.397	0.001	0.031
Cnpy3	1.844	0.008	0.063	*Prss12*	2.286	0.000	0.029
Cnst	1.991	0.017	0.085	*Prx*	1.489	0.001	0.033
Cops3	1.363	0.008	0.064	*Psmb11*	2.692	0.021	0.094
Coq10a	2.084	0.010	0.068	*Psmb7*	2.699	0.003	0.045
Cotl1	1.523	0.002	0.035	*Ptcd2*	1.699	0.016	0.085
Cox6b1	1.564	0.018	0.088	*Ptgds*	1.888	0.008	0.063
Cox7a2l	1.430	0.005	0.053	*Rab11fip5*	1.791	0.008	0.063
Cplx1	1.869	0.008	0.065	*Rab35*	1.527	0.008	0.063
Crip1	1.529	0.014	0.079	*Rab3ip*	1.739	0.005	0.053
Crispld2	1.532	0.006	0.056	*Rad54l*	1.412	0.018	0.088
Cspg5	1.427	0.010	0.069	*Rarres1*	1.432	0.001	0.031
Csrp2	2.150	0.001	0.030	*Rcor2*	1.946	0.006	0.056
Cst3	1.798	0.004	0.048	*Rep15*	3.803	0.006	0.059
Ctif	1.444	0.023	0.099	*Rhbdd2*	1.301	0.002	0.035
Ctnnbl1	1.636	0.019	0.089	*Rhot2*	1.367	0.013	0.076
Ctsf	1.591	0.000	0.029	*Rimklb*	1.410	0.021	0.094
Cyb5a	1.289	0.009	0.068	*Rnaseh2c*	2.276	0.010	0.069
Cyc1	3.399	0.002	0.034	*Rnf114*	1.743	0.001	0.029
Dbi	1.474	0.015	0.081	*Rnf121*	1.390	0.005	0.053
Dexi	2.255	0.000	0.026	*Rnf157*	1.611	0.005	0.055
Dffa	1.337	0.011	0.072	*Rom1*	2.221	0.000	0.032
Dhdh	4.211	0.008	0.064	*Rpl10a*	2.066	0.008	0.063
Dlg2	1.409	0.004	0.048	*Rprm*	1.661	0.004	0.048
Dnajb9	1.633	0.001	0.030	*Rps27*	2.271	0.023	0.099
Dnajc11	1.379	0.004	0.050	*S100a4*	1.233	0.003	0.045
Dnal4	1.470	0.019	0.090	*Sac3d1*	3.758	0.002	0.037
Dpm3	2.497	0.012	0.074	*Sap18*	1.448	0.024	0.100
Dpp9	1.459	0.007	0.061	*Sat1*	1.390	0.005	0.055
Eaf1	1.246	0.002	0.035	*Scg5*	1.738	0.011	0.072
Edf1	2.374	0.017	0.086	*Scn4b*	1.595	0.005	0.052
Efcc1	4.477	0.009	0.068	*Scrn1*	1.936	0.001	0.030
Egln2	1.685	0.001	0.031	*Scx*	2.374	0.004	0.049
Eif2b2	2.535	0.001	0.031	*Scyl3*	3.634	0.010	0.068
Eif3l	2.072	0.012	0.075	*Sec13*	2.615	0.017	0.086
Elp3	1.598	0.001	0.031	*Selm*	2.482	0.009	0.067
Eme1	1.587	0.009	0.068	*Sepp1*	2.699	0.002	0.035
Eme2	1.501	0.006	0.056	*Sfxn5*	1.714	0.003	0.046
Endod1	1.402	0.002	0.034	*Sh3bgr*	1.391	0.024	0.100
Enho	1.447	0.001	0.031	*Sh3gl2*	1.278	0.010	0.069
Eno2	1.548	0.020	0.092	*Sh3rf1*	1.571	0.002	0.038
Eny2	1.328	0.009	0.067	*Shd*	1.737	0.002	0.038
Epn3	1.200	0.014	0.079	*Sirt2*	1.287	0.004	0.050
Esrrg	1.705	0.007	0.063	*Slc22a17*	4.451	0.005	0.054
Etl4	1.537	0.005	0.052	*Slc25a25*	1.508	0.015	0.082
Fabp3	1.275	0.022	0.096	*Slc25a43*	3.074	0.021	0.095
Fabp7	3.165	0.002	0.038	*Slc25a5*	3.786	0.002	0.036
Faim2	1.328	0.002	0.034	*Slc38a10*	1.399	0.017	0.087
Fam160b2	1.237	0.015	0.083	*Slc4a2*	1.322	0.014	0.079
Fam162a	2.032	0.005	0.054	*Slc6a8*	1.844	0.008	0.063
Fam19a5	2.083	0.016	0.084	*Slc9a3r1*	2.002	0.004	0.051
Fam57b	2.035	0.005	0.054	*Slco2b1*	2.443	0.004	0.051
Fars2	1.969	0.002	0.038	*Smim1*	1.230	0.009	0.066
Fbxl12	1.201	0.006	0.057	*Smim4*	1.838	0.002	0.035
Fbxo27	2.483	0.001	0.031	*Smoc2*	1.302	0.004	0.049
Fbxo44	1.807	0.004	0.048	*Smox*	2.826	0.001	0.030
Fchsd1	1.429	0.005	0.053	*Smpx*	1.427	0.001	0.034
Fdx1l	1.385	0.018	0.088	*Sncb*	1.711	0.007	0.060
Fhdc1	1.306	0.000	0.026	*Snn*	2.308	0.012	0.074
Fkbp2	1.980	0.015	0.083	*Snx22*	2.722	0.009	0.068
Fkbp4	1.407	0.005	0.055	*Sphkap*	2.242	0.001	0.030
Fth1	4.168	0.000	0.022	*Sptb*	1.567	0.020	0.093

(*Table continues*)

Table 1. Continued

Genes	Log2 fold change	p	q	Genes	Log2 fold change	p	q
Fuca1	1.308	0.013	0.076	*Srm*	1.623	0.012	0.075
Gatb	1.370	0.008	0.064	*Stard3*	1.798	0.002	0.039
Glb1l2	2.686	0.001	0.031	*Stk32c*	1.467	0.022	0.096
Gle1	1.391	0.020	0.091	*Stmn4*	2.074	0.000	0.028
Glyr1	1.263	0.014	0.079	*Stxbp6*	1.486	0.024	0.100
Gps1	2.939	0.008	0.065	*Suclg1*	2.146	0.008	0.064
Gpx1	1.719	0.023	0.097	*Supt4a*	3.247	0.001	0.031
Grk6	1.513	0.007	0.061	*Suv420h1*	2.426	0.019	0.090
Gtf2h4	4.152	0.003	0.045	*Syn2*	1.312	0.001	0.030
Gtf2i	1.710	0.003	0.045	*Syne4*	2.723	0.002	0.037
Gtf2ird1	2.143	0.010	0.069	*Sys1*	1.933	0.003	0.046
Haghl	1.514	0.008	0.063	*Taf6l*	1.539	0.006	0.056
Hapln4	1.571	0.012	0.075	*Tango2*	1.243	0.008	0.065
Harbi1	1.772	0.011	0.070	*Tecr*	1.980	0.024	0.100
Haus8	3.145	0.010	0.069	*Tfb1m*	1.304	0.012	0.073
Hax1	1.463	0.007	0.063	*Thap11*	1.324	0.004	0.049
Hebp2	1.567	0.001	0.033	*Tifab*	1.602	0.018	0.088
Hhatl	2.106	0.003	0.045	*Timm9*	1.715	0.009	0.066
Hid1	1.773	0.013	0.077	*Tmco1*	1.240	0.014	0.079
Hist3h2ba	1.307	0.005	0.052	*Tmem101*	1.649	0.020	0.092
Hlcs	1.772	0.012	0.075	*Tmem126a*	1.893	0.001	0.030
Homer3	2.804	0.001	0.031	*Tmem132c*	2.205	0.007	0.059
Hpca	1.469	0.003	0.046	*Tmem14c*	1.461	0.022	0.096
Hs3st1	1.520	0.012	0.075	*Tmem18*	1.588	0.002	0.040
Hsdl2	1.375	0.005	0.053	*Tmem201*	1.336	0.001	0.030
Htra1	2.177	0.007	0.063	*Tmem203*	1.637	0.018	0.087
Hunk	3.047	0.007	0.061	*Tmem229b*	1.572	0.002	0.038
Iba57	1.357	0.014	0.080	*Tmem242*	1.386	0.018	0.088
Id3	2.405	0.005	0.053	*Tmem25*	2.039	0.001	0.030
Idh2	1.732	0.002	0.036	*Tmem258*	3.156	0.013	0.076
Idh3b	1.848	0.007	0.062	*Tmem60*	1.268	0.001	0.031
Imp3	2.481	0.007	0.060	*Tnfrsf1a*	1.468	0.005	0.055
Impdh2	1.694	0.004	0.051	*Tpbgl*	2.734	0.008	0.064
Inpp5j	2.890	0.006	0.058	*Trak1*	1.435	0.005	0.053
Itih5	1.235	0.006	0.058	*Trappc3*	2.247	0.020	0.093
Itm2c	1.551	0.002	0.035	*Trf*	2.565	0.002	0.037
Jam3	2.138	0.000	0.030	*Trp53rka*	1.316	0.001	0.030
Kat2a	1.756	0.009	0.067	*Tspan3*	1.262	0.012	0.074
Kcnq4	2.581	0.001	0.030	*Ttc9b*	1.870	0.011	0.071
Kctd15	2.542	0.016	0.084	*Txnl4b*	1.574	0.003	0.044
Krt10	1.758	0.008	0.064	*Tyr*	2.829	0.023	0.097
Lancl1	1.907	0.000	0.029	*Tyro3*	2.928	0.019	0.089
Laptm4b	1.441	0.001	0.031	*U2af1l4*	1.981	0.002	0.035
Ldhb	1.497	0.014	0.080	*Ube2v1*	1.615	0.006	0.058
Letm1	1.305	0.015	0.081	*Ubl5*	1.577	0.021	0.093
Lgi3	1.359	0.006	0.055	*Ufsp1*	2.295	0.001	0.034
Limd1	1.389	0.000	0.028	*Ulk1*	1.439	0.008	0.064
Lrp1	1.242	0.001	0.033	*Uqcc2*	2.331	0.006	0.058
Lyz2	3.211	0.002	0.040	*Uqcc3*	1.376	0.005	0.054
Lztr1	1.525	0.018	0.088	*Uqcrh*	1.253	0.016	0.084
Maged2	1.849	0.012	0.074	*Vasp*	1.204	0.024	0.100
Map1lc3b	1.800	0.001	0.030	*Vim*	1.384	0.007	0.060
Mark4	2.680	0.002	0.040	*Vwa7*	1.728	0.001	0.033
Mars	1.517	0.003	0.046	*Wbp1*	1.987	0.009	0.068
Mat2a	1.570	0.001	0.030	*Wfs1*	2.149	0.001	0.031
Meis2	1.776	0.004	0.051	*Wwox*	1.523	0.023	0.098
Mgat5	1.417	0.001	0.032	*Yif1a*	1.236	0.006	0.059
Mgst3	3.432	0.001	0.035	*Zfand2b*	2.929	0.005	0.054
Mief1	1.479	0.013	0.078	*Zfp180*	1.595	0.014	0.080
Mmd2	2.595	0.003	0.044	*Zfp335*	1.645	0.017	0.085
Mobp	1.996	0.015	0.082	*Zfp771*	1.604	0.023	0.097
Mpc2	1.877	0.004	0.052				

Table 2. Genes upregulated in the DRG input

Genes	Log2 fold change	p	q	Genes	Log2 fold change	p	q
1700019D03Rik	−1.367	0.001	0.030	*Mpped2*	−2.004	0.000	0.026
9330159F19Rik	−1.337	0.001	0.031	*Mpv17l2*	−1.509	0.006	0.055
9330182L06Rik	−1.668	0.006	0.056	*Mt-Co3*	−1.553	0.007	0.063
Abca5	−1.456	0.008	0.063	*Myc*	−1.925	0.001	0.030
Acacb	−1.267	0.010	0.070	*Myh1*	−4.915	0.002	0.037
Acbd5	−1.220	0.018	0.088	*Myl1*	−7.949	0.000	0.022
Acpp	−1.662	0.000	0.022	*Myo1b*	−1.242	0.004	0.049
Acsl4	−1.505	0.000	0.025	*Myom1*	−2.336	0.002	0.038
Acta1	−6.161	0.000	0.027	*Myt1l*	−1.439	0.005	0.055
Actn1	−1.467	0.002	0.036	*Nectin1*	−1.609	0.010	0.069
Adcyap1	−1.814	0.003	0.045	*Nedd4l*	−1.349	0.001	0.029
Adgrd1	−1.531	0.006	0.057	*Nek1*	−1.475	0.017	0.086
Adgrf5	−1.678	0.004	0.049	*Nfya*	−1.752	0.018	0.087
Adk	−2.250	0.000	0.026	*Nhs*	−1.233	0.001	0.031
Agtr1a	−2.244	0.002	0.038	*Nktr*	−1.403	0.008	0.063
Ammecr1	−1.266	0.012	0.074	*Noct*	−1.573	0.015	0.082
Ank3	−1.585	0.000	0.029	*Nptx2*	−1.297	0.002	0.040
Ankrd6	−1.453	0.003	0.043	*Nptxr*	−1.481	0.001	0.031
Ano3	−1.205	0.003	0.044	*Npy2r*	−2.372	0.007	0.061
Arfgef2	−1.305	0.000	0.026	*Nras*	−1.633	0.012	0.075
Arhgap23	−1.415	0.012	0.074	*Nrip1*	−1.304	0.000	0.027
Arhgap26	−2.827	0.000	0.026	*Nrxn3*	−1.701	0.008	0.064
Arrdc3	−1.213	0.023	0.099	*Nt5e*	−2.145	0.001	0.034
Ass1	−1.757	0.002	0.040	*Nup88*	−1.244	0.023	0.098
Astn1	−1.500	0.007	0.061	*Ocrl*	−1.219	0.004	0.049
Atp2b4	−2.126	0.001	0.030	*Ormdl1*	−1.558	0.004	0.048
Auts2	−1.836	0.000	0.027	*Osbpl3*	−1.696	0.000	0.026
B630005N14Rik	−1.380	0.017	0.086	*Pabpc1*	−1.654	0.020	0.093
Bdnf	−1.450	0.003	0.042	*Pabpn1*	−1.450	0.009	0.067
Bnc2	−1.401	0.004	0.050	*Palm2*	−2.056	0.005	0.055
Brms1l	−1.357	0.012	0.073	*Palmd*	−1.212	0.000	0.026
Cacna2d1	−1.978	0.000	0.039	*Pam*	−1.491	0.006	0.057
Camk2a	−1.912	0.001	0.031	*Panx1*	−1.364	0.002	0.040
Camk2d	−1.608	0.011	0.071	*Paqr3*	−1.230	0.006	0.058
Camta1	−1.640	0.013	0.077	*Pde10a*	−1.289	0.001	0.030
Capn1	−1.429	0.003	0.042	*Pde11a*	−1.938	0.000	0.021
Car8	−1.627	0.011	0.072	*Pdlim1*	−1.524	0.005	0.052
Casz1	−1.381	0.004	0.048	*Pfkp*	−1.296	0.004	0.052
Ccdc141	−1.908	0.002	0.035	*Pfn1*	−2.156	0.001	0.030
Cct8	−1.364	0.009	0.068	*Pgm2l1*	−1.494	0.000	0.029
Cd274	−1.797	0.005	0.052	*Phip*	−1.266	0.004	0.050
Cd2ap	−1.457	0.012	0.074	*Pitpnc1*	−1.209	0.000	0.026
Cd44	−1.559	0.001	0.030	*Pitpnm2*	−1.297	0.015	0.080
Cd47	−1.588	0.000	0.020	*Pkia*	−1.817	0.003	0.042
Cd55	−2.309	0.001	0.031	*Plcb3*	−1.560	0.000	0.025
Cdc14b	−1.372	0.000	0.025	*Plekha6*	−1.243	0.008	0.064
Celf4	−1.240	0.005	0.052	*Plvap*	−1.298	0.018	0.087
Celf6	−1.775	0.013	0.077	*Plxnc1*	−1.740	0.005	0.053
Cep170	−1.468	0.006	0.058	*Plxnd1*	−1.345	0.002	0.035
Cfap157	−1.378	0.002	0.040	*Polr2a*	−1.357	0.001	0.031
Chml	−1.782	0.012	0.074	*Pou1f1*	−2.038	0.019	0.089
Chpt1	−1.408	0.010	0.068	*Ppef1*	−1.257	0.004	0.049
Ciapin1	−1.263	0.020	0.093	*Ppp1r12a*	−1.564	0.001	0.030
Ckm	−7.336	0.001	0.031	*Ppp3ca*	−1.498	0.000	0.021
Clgn	−1.231	0.009	0.067	*Ppp6c*	−1.218	0.010	0.068
Clip2	−2.335	0.003	0.046	*Prdm8*	−2.355	0.001	0.030
Cmip	−1.580	0.002	0.037	*Prg2*	−3.717	0.001	0.030
Cnot1	−1.720	0.000	0.025	*Prkag2*	−1.331	0.022	0.097
Cnot4	−1.280	0.004	0.048	*Prkar2b*	−1.651	0.000	0.025
Cntrl	−1.361	0.004	0.050	*Prkca*	−2.159	0.000	0.025
Cpeb1	−1.200	0.005	0.053	*Ptgdr*	−1.577	0.002	0.035
Cpne2	−1.790	0.018	0.087	*Ptger1*	−1.387	0.008	0.063
Cpsf7	−1.260	0.010	0.069	*Ptms*	−1.523	0.000	0.026
Csrnp3	−1.215	0.000	0.025	*Ptprt*	−2.355	0.001	0.029

(*Table continues*)

Table 2. Continued

Genes	Log2 fold change	p	q	Genes	Log2 fold change	p	q
Ctsl	−1.450	0.002	0.034	*Ptrf*	−1.688	0.002	0.040
Ddx3x	−1.330	0.001	0.030	*Pum1*	−1.405	0.008	0.065
Deptor	−1.652	0.001	0.033	*Pura*	−1.301	0.006	0.056
Dgkh	−1.341	0.005	0.055	*Purb*	−1.209	0.021	0.095
Dgkz	−1.775	0.000	0.024	*Pygl*	−1.338	0.001	0.031
Disp2	−1.423	0.010	0.069	*Rab27b*	−1.526	0.016	0.083
Dpp10	−1.486	0.000	0.021	*Rab39b*	−1.515	0.003	0.045
Dpp6	−1.293	0.002	0.039	*Rab3c*	−1.439	0.013	0.075
Ebf3	−1.919	0.002	0.035	*Rabgap1l*	−1.317	0.003	0.044
Eif4e3	−1.421	0.001	0.032	*Raph1*	−1.327	0.007	0.060
Etnk1	−1.896	0.001	0.030	*Rasgrp1*	−1.547	0.001	0.031
F2rl2	−1.621	0.012	0.075	*Rbms1*	−1.558	0.002	0.034
Fabp4	−5.383	0.000	0.026	*Reps2*	−1.310	0.003	0.041
Fam102b	−1.588	0.000	0.025	*Rgmb*	−1.207	0.015	0.082
Fam122b	−2.137	0.004	0.050	*Rgs17*	−2.168	0.000	0.026
Fam179b	−1.540	0.003	0.041	*Rnf144a*	−1.423	0.000	0.029
Fam214b	−1.405	0.001	0.031	*Robo2*	−1.321	0.001	0.030
Fam222b	−1.668	0.007	0.062	*Rps11*	−1.411	0.005	0.055
Filip1	−1.223	0.001	0.030	*Rspo2*	−1.809	0.000	0.026
Fsd2	−2.160	0.012	0.073	*Runx1*	−1.204	0.006	0.055
Gal	−2.045	0.002	0.035	*Ryr1*	−3.459	0.010	0.069
Ghr	−2.439	0.004	0.049	*S100a11*	−2.366	0.007	0.063
Gm17305	−1.767	0.003	0.046	*S100a8*	−3.282	0.001	0.029
Gm42417	−4.801	0.000	0.029	*S100a9*	−4.220	0.000	0.021
Gmfb	−1.259	0.004	0.049	*Safb*	−1.574	0.011	0.070
Gna14	−1.468	0.021	0.095	*Samsn1*	−2.440	0.001	0.030
Gnai3	−1.748	0.011	0.072	*Scd1*	−1.809	0.001	0.034
Gnao1	−1.462	0.001	0.032	*Scg2*	−1.809	0.009	0.066
Gnaq	−1.531	0.002	0.034	*Scg3*	−1.743	0.002	0.038
Gnb4	−1.236	0.008	0.064	*Scn9a*	−1.579	0.000	0.027
Gp1bb	−1.271	0.020	0.093	*Scyl2*	−1.375	0.001	0.031
Grip1	−1.423	0.013	0.076	*Sdcbp*	−1.233	0.001	0.030
Grm7	−1.784	0.001	0.033	*Sema4b*	−1.437	0.002	0.039
H2-K1	−1.611	0.019	0.091	*Sepw1*	−1.253	0.013	0.077
Hace1	−1.481	0.008	0.065	*Slc16a3*	−2.036	0.001	0.029
Hba-a2	−1.762	0.004	0.052	*Slc27a3*	−1.610	0.008	0.065
Hbb-bt	−1.668	0.004	0.052	*Slc35a5*	−1.304	0.000	0.038
Hcn3	−1.929	0.003	0.045	*Slc37a1*	−1.336	0.016	0.085
Hgf	−1.762	0.003	0.044	*Slc39a6*	−1.502	0.003	0.041
Hmbox1	−1.450	0.011	0.072	*Slc51a*	−1.622	0.002	0.035
Hmgcl	−1.314	0.013	0.077	*Slc5a3*	−1.415	0.014	0.080
Hoxa10	−7.016	0.000	0.020	*Slc9a6*	−1.278	0.002	0.039
Hoxa7	−7.044	0.000	0.045	*Smim10l1*	−1.212	0.002	0.036
Hoxa9	−6.931	0.000	0.027	*Smim5*	−1.524	0.015	0.080
Hoxb2	−5.272	0.001	0.029	*Socs2*	−1.430	0.001	0.031
Hoxb4	−6.121	0.000	0.026	*Sorl1*	−1.403	0.002	0.034
Hoxb5	−6.619	0.000	0.020	*Spred2*	−1.203	0.008	0.064
Hoxb9	−9.266	0.000	0.024	*Spryd7*	−1.357	0.010	0.068
Hoxc6	−11.922	0.000	0.024	*Srek1*	−1.309	0.009	0.067
Hoxd10	−11.238	0.000	0.023	*Ssbp3*	−1.358	0.008	0.064
Hoxd4	−2.142	0.003	0.046	*St8sia3*	−1.270	0.007	0.060
Hoxd8	−1.603	0.004	0.048	*Stag2*	−1.202	0.005	0.053
Hoxd9	−3.929	0.001	0.030	*Sycp3*	−1.430	0.019	0.089
Hs6st2	−2.118	0.004	0.050	*Synpr*	−1.887	0.001	0.029
Hsp90ab1	−1.392	0.006	0.056	*Syt1*	−1.331	0.000	0.021
Idh1	−2.275	0.000	0.047	*Syt4*	−2.148	0.004	0.052
Idi1	−1.751	0.022	0.097	*Syt7*	−1.673	0.001	0.029
Ids	−1.571	0.009	0.067	*Syt9*	−1.899	0.000	0.026
Il10rb	−1.208	0.020	0.093	*Tac1*	−1.726	0.000	0.028
Il6st	−1.838	0.001	0.030	*Taf1*	−1.263	0.024	0.100
Impad1	−1.490	0.002	0.035	*Taok1*	−1.691	0.005	0.055
Ina	−2.171	0.000	0.028	*Tlx3*	−1.349	0.001	0.030
Irf2	−1.226	0.000	0.029	*Tmem158*	−1.431	0.003	0.045
Izumo4	−1.366	0.009	0.068	*Tmem164*	−1.228	0.008	0.063

(*Table continues*)

Table 2. Continued

Genes	Log2 fold change	p	q	Genes	Log2 fold change	p	q
Kcna4	−1.408	0.010	0.069	*Tmem185b*	−1.358	0.019	0.088
Kcnab1	−1.296	0.003	0.046	*Tmem200a*	−1.785	0.003	0.041
Kcnb2	−2.196	0.001	0.032	*Tmem233*	−1.233	0.019	0.089
Kcnt1	−1.215	0.017	0.086	*Tmem255a*	−1.367	0.001	0.033
Kdelc2	−1.279	0.010	0.070	*Tmem56*	−1.466	0.009	0.068
Kdm7a	−1.460	0.009	0.068	*Tmtc2*	−1.914	0.015	0.082
Kif5b	−1.301	0.008	0.064	*Tmx3*	−1.230	0.008	0.064
Klf7	−1.346	0.000	0.026	*Tnnc2*	−6.667	0.001	0.030
Larp1	−1.374	0.006	0.056	*Tnnt3*	−7.079	0.000	0.028
Lbh	−1.629	0.003	0.042	*Top2a*	−1.930	0.008	0.064
Lcor	−1.431	0.008	0.063	*Tra2a*	−1.451	0.015	0.081
Ldb2	−1.834	0.001	0.031	*Trp53bp1*	−1.257	0.004	0.049
Ldlr	−1.708	0.002	0.034	*Trpc3*	−1.616	0.012	0.073
Lifr	−1.742	0.005	0.052	*Trpv1*	−2.016	0.008	0.065
Lonrf1	−1.453	0.002	0.035	*Ubb*	−1.257	0.022	0.097
Lox	−2.537	0.018	0.087	*Ubqln2*	−1.407	0.004	0.050
Lpar3	−1.721	0.003	0.046	*Ugcg*	−1.398	0.007	0.060
Lrfn1	−1.409	0.000	0.022	*Unc13c*	−1.455	0.002	0.037
Lrrc8b	−1.402	0.001	0.030	*Usp17la*	−1.946	0.011	0.072
Lrrtm2	−1.389	0.018	0.088	*Usp9x*	−1.500	0.011	0.072
Ly86	−2.557	0.009	0.068	*Vwa5a*	−1.352	0.002	0.040
Magi3	−1.665	0.001	0.030	*Wasf1*	−1.501	0.000	0.020
Mal2	−2.994	0.000	0.029	*Wfdc2*	−1.246	0.019	0.090
Mb	−6.746	0.000	0.027	*Xirp2*	−8.656	0.000	0.026
Mbnl1	−1.392	0.018	0.088	*Yod1*	−1.273	0.009	0.067
Mbnl2	−1.795	0.000	0.029	*Zbtb44*	−1.315	0.015	0.080
Mcoln1	−1.305	0.010	0.070	*Zdhhc13*	−1.497	0.000	0.028
Mfsd7b	−1.521	0.007	0.062	*Zeb2*	−1.453	0.011	0.070
Mon1a	−1.310	0.000	0.029	*Zfhx2*	−1.542	0.016	0.084
				Zfhx3	−1.317	0.007	0.060

2 PCs (PC1 = difference between DRG and TG transcriptomes; and PC2 = difference between the DRG and TG Nav1.8-TRAP translatomes) explained the majority of the variance seen in the dataset (Fig. 3*B*). Further clustering analysis confirmed the findings of the PC analysis (Fig. 3*C*).

Analysis of the input transcriptome data between TG and DRG revealed that 379 genes were significantly enriched in the TG and 315 in the DRG (Fig. 4*A*; Tables 1, 2). Among these 315 genes in the DRG, we observed enrichment of the *Hox* family transcription factors (Fig. 4*A*). These genes are well-known regulators of rostral to caudal segmental development, so enrichment in DRG is expected given the rostral–caudal extent of the DRG (Kammermeier and Reichert, 2001). Among the 379 genes enriched in the TG, we found particularly high expression and enrichment of *Fth1* and *Pak1* (Fig. 4*A*). Analysis of the Nav1.8-TRAP dataset revealed 372 genes enriched in the TG and 348 in the DRG (Fig. 4*A*; Tables 3, 4). Consistent with the transcriptome results, the *Hox* genes showed a highly enriched translational profile in the DRG (Fig. 4*A*). Among the top mRNAs highly associated with ribosomes in the TG Nav1.8-TRAP dataset, we found *Nme3*, *Il1rl2*, and *Edf1* (Fig. 4*A*). None of these 3 genes has been associated with a specific TG function previously, although the *Il1rl2* gene encodes a receptor for interleukin 1β (IL1β), which activates TG nociceptors through a mechanism that has previously been attributed to IL1β Type 1 receptors (Takeda et al., 2008). GO term analysis of the differentially expressed genes in the Nav1.8-TRAP datasets revealed an enrichment in specific pathways, including VEGFR, FGFR, as well as the PI3K-mTOR pathway (Fig. 4*B*). Interestingly, we observed an enrichment in AMP-activated protein kinase (AMPK)-related genes in the

Table 3. Genes upregulated in the TG Nav1.8-TRAP dataset

Genes	Log2 fold change	*p*	*q*	Genes	Log2 fold change	*p*	*q*
0610009B22Rik	3.295	0.001	0.031	*Nap1l5*	2.348	0.001	0.029
1110032A03Rik	2.542	0.007	0.059	*Nbea*	2.525	0.001	0.028
1110065P20Rik	5.685	0.001	0.032	*Nbl1*	2.738	0.015	0.085
1700037C18Rik	2.913	0.010	0.072	*Ndel1*	3.132	0.000	0.010
2010107E04Rik	2.008	0.000	0.016	*Ndufa1*	2.495	0.002	0.034
2210013O21Rik	2.570	0.006	0.056	*Ndufb2*	3.065	0.002	0.034
2700094K13Rik	3.894	0.004	0.049	*Ndufb5*	2.214	0.001	0.027
9430016H08Rik	3.239	0.016	0.089	*Ndufb9*	2.915	0.000	0.017
Aard	7.736	0.005	0.050	*Ndufs2*	2.315	0.003	0.043
Acp1	2.522	0.004	0.049	*Ngfr*	2.166	0.011	0.075
Adam9	4.085	0.004	0.045	*Nme3*	11.466	0.000	0.020
Adra2c	5.673	0.001	0.025	*Nrn1l*	4.040	0.009	0.068
Akirin1	2.298	0.009	0.068	*Nsun3*	3.157	0.018	0.093
Akt1	3.554	0.006	0.058	*Nt5m*	3.252	0.017	0.090
Alkbh3	7.497	0.002	0.035	*Nubp2*	5.238	0.007	0.063
Amacr	5.927	0.013	0.082	*Nudt10*	4.615	0.010	0.072
Anapc13	3.962	0.015	0.087	*Nudt11*	3.346	0.018	0.093
Ankrd24	2.576	0.012	0.078	*Nudt7*	4.780	0.002	0.037
Anxa5	2.142	0.004	0.047	*Nup37*	4.108	0.000	0.017
Apip	7.421	0.003	0.042	*Ost4*	2.585	0.004	0.050
Apln	4.200	0.009	0.069	*Ostf1*	2.376	0.003	0.042
Arl5a	2.178	0.002	0.038	*Pacsin1*	2.217	0.016	0.089
Arl6	4.831	0.003	0.042	*Pak1*	5.331	0.006	0.056
Arl8a	2.045	0.008	0.066	*Pak3*	3.228	0.009	0.069
Armc1	2.080	0.016	0.089	*Parp3*	2.863	0.010	0.072
Arpc1b	3.965	0.000	0.020	*Pcbd2*	3.529	0.002	0.037
Arpc5l	2.223	0.002	0.039	*Pcolce2*	3.567	0.003	0.042
Asna1	3.806	0.010	0.073	*Pcp4l1*	3.151	0.004	0.045
Atg4c	4.484	0.001	0.028	*Pcsk1n*	2.681	0.010	0.072
Atox1	2.116	0.010	0.072	*Pcsk7*	4.142	0.005	0.050
Atp5c1	2.674	0.003	0.040	*Pdcd6*	2.770	0.009	0.067
Atp5d	2.552	0.006	0.058	*Pde6d*	5.181	0.004	0.050
Atp5g1	2.613	0.003	0.040	*Pdlim2*	3.067	0.001	0.027
Atp5s	6.255	0.000	0.018	Pdzd9	2.834	0.005	0.050
Atp6v0d1	3.072	0.000	0.018	*Pex11b*	7.187	0.000	0.003
Avpi1	2.049	0.005	0.053	*Pfdn1*	2.368	0.013	0.082
Banf1	2.411	0.001	0.028	*Pfkm*	2.196	0.011	0.074
Bbs9	4.103	0.021	0.099	*Phospho2*	2.332	0.013	0.082
Bloc1s1	2.178	0.015	0.085	*Phpt1*	2.748	0.007	0.063
Bloc1s3	4.164	0.003	0.042	*Pigh*	2.609	0.011	0.075
Btbd2	2.239	0.002	0.036	*Pin1*	3.518	0.001	0.031
C77080	3.683	0.000	0.016	*Pla2g16*	2.041	0.017	0.091
Cacng7	2.455	0.005	0.054	*Plekhb1*	3.646	0.014	0.083
Calca	2.290	0.001	0.027	*Plpp1*	4.280	0.017	0.091
Calm2	2.036	0.014	0.085	*Pole3*	3.127	0.020	0.097
Camk2g	2.396	0.003	0.044	*Polr2d*	6.787	0.000	0.004
Cbln1	6.228	0.004	0.047	*Polr2j*	6.438	0.001	0.027
Ccdc88a	2.029	0.007	0.059	*Polr2l*	2.072	0.011	0.076
Cdc123	2.146	0.020	0.098	*Polr2m*	2.330	0.005	0.050
Cdk2ap1	4.137	0.003	0.040	*Pomgnt1*	3.461	0.020	0.099
Cdkn1b	2.713	0.001	0.024	*Ppm1j*	2.163	0.009	0.067
Cdr2l	2.794	0.007	0.061	*Ppp2r5c*	2.205	0.014	0.084
Cebpzos	3.122	0.004	0.049	*Praf2*	2.266	0.019	0.096
Cela1	4.351	0.004	0.049	*Prkcd*	2.054	0.003	0.040
Cenpq	4.971	0.002	0.037	*Prkcdbp*	6.444	0.002	0.035
Cfap69	3.913	0.012	0.077	*Prkrir*	2.325	0.008	0.064
Cfl1	2.008	0.001	0.032	*Prorsd1*	5.144	0.008	0.065
Chchd1	3.792	0.000	0.017	*Psma1*	2.561	0.017	0.091
Chchd10	3.927	0.011	0.074	*Psmb11*	2.717	0.000	0.021
Chchd4	2.146	0.003	0.040	*Psmc3ip*	6.150	0.007	0.061
Chd3os	2.704	0.003	0.040	*Qars*	2.763	0.012	0.079
Chmp6	2.299	0.021	0.099	*Rab10*	2.106	0.010	0.071
Chodl	5.030	0.016	0.089	*Rab15*	3.719	0.013	0.080
Chp1	4.425	0.000	0.017	*Rab1a*	4.034	0.008	0.064

(*Table continues*)

Table 3. Continued

Genes	Log2 fold change	*p*	*q*	Genes	Log2 fold change	*p*	*q*
Clmp	2.253	0.019	0.094	*Rab28*	2.269	0.001	0.032
Cnih2	4.508	0.007	0.061	*Rab33a*	3.270	0.015	0.085
Cnrip1	2.211	0.008	0.066	*Rab35*	2.067	0.012	0.078
Commd1	3.042	0.003	0.045	*Rab4b*	2.707	0.008	0.065
Commd4	2.980	0.019	0.094	*Rad54l*	5.057	0.001	0.026
Coq3	3.088	0.011	0.075	*Rad9b*	2.382	0.012	0.079
Cox6b1	2.708	0.000	0.023	*Rho*	4.096	0.003	0.040
Cox7a2	2.299	0.006	0.056	*Rhog*	4.929	0.012	0.078
Cox7b	4.295	0.000	0.017	*Rnase4*	2.128	0.018	0.092
Cox7c	2.255	0.001	0.028	*Rnf114*	3.644	0.013	0.082
Cox8a	2.576	0.000	0.021	*Rnf215*	4.125	0.006	0.058
Crlf2	3.905	0.011	0.075	*Rnf7*	2.072	0.013	0.081
Crtc2	5.091	0.001	0.023	*Romo1*	2.456	0.000	0.021
Crtc3	3.703	0.018	0.092	*Rpl10*	3.076	0.013	0.080
Ctxn3	2.686	0.000	0.023	*Rpl28*	2.167	0.019	0.095
Cyb5a	2.330	0.012	0.079	*Rpl29*	5.333	0.021	0.099
Cyc1	3.989	0.013	0.080	*Rpl35*	3.039	0.003	0.040
Cystm1	3.446	0.002	0.038	*Rpl37*	2.967	0.003	0.042
Dad1	4.088	0.006	0.056	*Rpl39*	3.241	0.001	0.027
Dalrd3	7.942	0.002	0.036	*Rps23*	2.219	0.020	0.097
Dda1	2.393	0.017	0.091	*Rps29*	2.912	0.002	0.037
Dlg2	4.233	0.010	0.072	*Rpusd1*	3.617	0.008	0.064
Dnajc12	3.352	0.016	0.088	*Rraga*	2.131	0.000	0.023
Dnal4	4.100	0.012	0.076	*Rtn4r*	2.805	0.001	0.028
Dpep2	4.510	0.001	0.026	*Rxrg*	4.463	0.004	0.049
Dpm3	3.461	0.019	0.095	*Sac3d1*	4.162	0.009	0.070
Dzank1	3.857	0.011	0.074	*Sap18*	3.653	0.019	0.095
Edf1	2.907	0.000	0.002	*Sdhb*	4.145	0.013	0.082
Eef1a1	2.126	0.016	0.088	*Sdhd*	2.350	0.008	0.066
Efcc1	5.725	0.001	0.032	*Sec13*	5.366	0.002	0.037
Eif4a3	2.748	0.008	0.066	*Sec23ip*	2.817	0.014	0.083
Emb	2.251	0.000	0.017	*Sep15*	2.455	0.009	0.068
Enox1	3.300	0.017	0.090	*Sepp1*	2.412	0.013	0.081
Epm2a	2.756	0.003	0.041	*Serp2*	3.709	0.004	0.046
Esyt1	4.806	0.004	0.045	*Serping1*	4.031	0.007	0.060
Exd2	5.752	0.000	0.016	*Sh2d3c*	3.339	0.019	0.095
Exosc6	4.476	0.005	0.053	*Sh3bgrl*	2.659	0.004	0.049
Fabp7	3.901	0.001	0.024	*Sh3bgrl3*	2.229	0.001	0.032
Fam105a	3.610	0.013	0.082	*Shd*	8.734	0.007	0.061
Fam188a	2.065	0.011	0.075	*Shisa5*	2.629	0.011	0.074
Fam58b	3.355	0.002	0.036	*Sirt2*	3.344	0.020	0.098
Fam89a	3.170	0.010	0.072	*Sirt3*	3.145	0.017	0.090
Far2	3.913	0.006	0.056	*Sla2*	2.598	0.002	0.037
Farp1	6.925	0.000	0.016	*Slc22a17*	3.985	0.018	0.092
Fbxl16	2.675	0.007	0.060	*Slc24a2*	2.209	0.001	0.028
Fbxo2	3.859	0.007	0.063	*Slc25a3*	3.404	0.006	0.058
Fbxo27	8.071	0.000	0.023	*Slc25a43*	2.557	0.019	0.095
Fgf9	4.057	0.007	0.063	*Slc35d2*	6.734	0.000	0.018
Fgfr2	6.744	0.003	0.043	*Slc3a2*	3.247	0.001	0.025
Fhl1	2.487	0.001	0.024	*Slc45a4*	2.344	0.009	0.068
Fkbp2	2.064	0.008	0.065	*Slc46a3*	5.451	0.003	0.040
Fsd1	2.330	0.010	0.072	*Slc6a15*	3.041	0.014	0.084
Fth1	3.259	0.001	0.023	*Slco2b1*	5.287	0.004	0.047
Fxyd6	2.042	0.006	0.056	*Slitrk1*	3.031	0.018	0.094
Gabrg1	3.806	0.000	0.018	*Smdt1*	2.724	0.000	0.019
Galnt18	2.412	0.013	0.080	*Smim12*	2.038	0.000	0.021
Gatad1	2.512	0.004	0.047	*Smim8*	2.292	0.003	0.042
Gipc1	3.901	0.018	0.093	*Snapc5*	2.360	0.016	0.088
Glb1l2	4.152	0.008	0.066	*Snn*	3.703	0.015	0.085
Gm15440	5.964	0.012	0.079	*Snrpb*	2.974	0.002	0.037
Gm5113	6.649	0.001	0.032	*Snrpn*	3.974	0.002	0.037
Gmnn	4.878	0.001	0.026	*Snx3*	2.491	0.002	0.037
Gng5	4.458	0.000	0.018	*Spcs1*	2.441	0.021	0.099
Gng8	4.700	0.006	0.057	*Spon1*	3.949	0.021	0.099

(*Table continues*)

Table 3. Continued

Genes	Log2 fold change	p	q	Genes	Log2 fold change	p	q
Golga1	3.883	0.016	0.089	*Srp14*	2.998	0.000	0.021
Gpr35	3.338	0.017	0.091	Ssr4	3.347	0.011	0.075
Gramd1b	2.251	0.000	0.020	*Stau2*	2.158	0.008	0.066
Grpel2	3.678	0.018	0.092	*Strada*	5.449	0.008	0.064
Gtf2i	3.014	0.011	0.075	*Stx2*	3.170	0.000	0.017
H2-T23	4.183	0.010	0.070	*Suclg1*	2.738	0.010	0.073
H2afz	2.207	0.003	0.042	*Supt4a*	3.527	0.001	0.032
Hist3h2ba	2.569	0.016	0.089	*Tagln3*	3.422	0.004	0.047
Hsbp1	2.142	0.016	0.089	*Tbc1d14*	2.192	0.009	0.070
Idh3b	3.457	0.001	0.025	*Tfb1m*	3.745	0.013	0.082
Ift122	3.334	0.011	0.074	*Thoc7*	2.488	0.008	0.066
Ift20	2.144	0.021	0.099	*Tifab*	5.602	0.004	0.045
Ift43	6.053	0.018	0.094	*Timm8b*	4.092	0.007	0.061
Igsf21	4.754	0.014	0.084	*Tjap1*	3.096	0.021	0.099
Il1rl2	8.506	0.000	0.016	*Tmem106b*	2.653	0.011	0.076
Imp3	2.343	0.001	0.032	*Tmem199*	4.071	0.014	0.084
Inpp5j	4.481	0.008	0.064	*Tmem216*	8.212	0.001	0.026
Isca2	2.096	0.011	0.074	*Tmem230*	2.058	0.006	0.058
Iscu	3.142	0.006	0.058	*Tmem258*	5.441	0.000	0.017
Kcnip1	5.122	0.001	0.032	*Tmem53*	3.911	0.009	0.069
Kcnip4	2.177	0.002	0.038	*Tmem62*	4.157	0.014	0.083
Kctd8	2.176	0.006	0.055	*Tnfrsf1a*	5.108	0.008	0.065
Klf8	4.565	0.004	0.047	*Tnfsfm13*	5.814	0.015	0.085
Lamtor5	2.577	0.005	0.055	*Tomm7*	2.169	0.000	0.017
Lcmt1	2.326	0.006	0.056	*Tpd52l1*	4.373	0.009	0.068
Lgals3bp	6.428	0.008	0.064	*Tpgs2*	3.087	0.004	0.049
Limk1	2.887	0.002	0.034	*Tppp3*	2.673	0.000	0.015
Lipa	2.672	0.005	0.054	*Trappc1*	3.056	0.019	0.095
Lix1	2.853	0.002	0.035	*Trdmt1*	5.930	0.000	0.021
Lrrc8a	2.077	0.000	0.018	*Triap1*	2.123	0.008	0.064
Ltbr	3.603	0.007	0.063	*Trim12a*	2.989	0.011	0.075
Lxn	2.922	0.001	0.026	*Trim9*	3.505	0.014	0.084
Lyrm2	4.541	0.000	0.023	*Trnp1*	2.255	0.003	0.040
Lyrm5	2.559	0.019	0.095	*Tspan17*	5.060	0.008	0.066
M6pr	2.171	0.007	0.062	*Tspan3*	2.352	0.003	0.040
Manbal	2.620	0.009	0.069	*Tspan7*	2.270	0.001	0.027
Map1lc3b	2.978	0.001	0.028	*Tub*	6.954	0.000	0.016
Mapkap1	2.645	0.010	0.070	*Tubb4b*	2.426	0.002	0.037
Mapkapk5	2.476	0.004	0.045	*Tyro3*	5.176	0.000	0.023
Mast2	4.666	0.004	0.049	*Ubald1*	3.325	0.003	0.040
Mbd2	3.693	0.012	0.078	*Ubl5*	2.981	0.006	0.058
Mblac2	3.198	0.007	0.063	*Ulk1*	2.369	0.009	0.067
Mboat7	4.459	0.005	0.055	*Uqcrb*	3.669	0.001	0.025
Mgst3	5.093	0.004	0.046	*Uqcrfs1*	2.994	0.005	0.052
Mid2	6.101	0.001	0.028	*Usmg5*	3.313	0.001	0.027
Minpp1	4.786	0.004	0.047	*Vkorc1l1*	3.000	0.010	0.072
Mipol1	3.394	0.015	0.086	*Vta1*	2.955	0.012	0.076
Mlf2	2.377	0.000	0.018	*Vwc2l*	3.597	0.010	0.071
Mob3b	3.803	0.020	0.099	*Wbp1*	4.041	0.019	0.095
Mrpl18	2.783	0.000	0.023	*Wbp2*	2.195	0.000	0.002
Mrpl27	2.877	0.013	0.081	*Wdr59*	3.560	0.004	0.049
Mrps14	4.314	0.004	0.049	*Wfs1*	4.090	0.009	0.067
Mrps36	4.605	0.006	0.058	*Wisp1*	5.770	0.008	0.064
Msra	3.657	0.013	0.082	*Ypel3*	2.511	0.003	0.042
mt-Nd2	2.268	0.007	0.063	*Ywhaq*	2.191	0.001	0.026
Mxd3	2.495	0.007	0.060	*Zdhhc6*	4.565	0.008	0.064
Mzt1	2.130	0.000	0.021	*Zfp932*	3.625	0.020	0.097
Naa38	4.005	0.018	0.093	*Zfp944*	6.108	0.006	0.056

DRG-TRAP dataset (Fig. 4*B*). This finding is intriguing because the AMPK pathway is a negative regulator of PI3K-mTOR signaling (Hardie, 2014, 2015) and suggests shifting in the balance between these two signaling pathways between the DRG and TG.

Table 4. Genes upregulated in the DRG Nav1.8-TRAP dataset

Genes	Log2 fold change	p	q	Genes	Log2 fold change	p	q
2810417H13Rik	−7.030	0.002	0.036	*Mif*	−2.343	0.012	0.078
A430078G23Rik	−4.575	0.005	0.055	*Mmp15*	−2.137	0.005	0.055
Abca6	−10.621	0.000	0.017	*Mon1a*	−2.894	0.002	0.037
Abhd17c	−2.949	0.000	0.017	*Mrpl14*	−3.067	0.020	0.099
Abt1	−2.637	0.008	0.065	*Mrpl37*	−2.040	0.003	0.044
Acaca	−2.654	0.002	0.037	*Mrto4*	−3.186	0.006	0.056
Acacb	−3.534	0.005	0.055	*Msn*	−2.617	0.003	0.040
Acot6	−7.991	0.001	0.029	*Mt-Co3*	−6.804	0.001	0.026
Acta1	−5.881	0.006	0.057	*Mterf4*	−2.725	0.009	0.068
Actb	−2.404	0.000	0.016	*Mvd*	−2.888	0.002	0.035
Adap1	−2.420	0.010	0.073	*Myc*	−6.466	0.001	0.030
Adgrb3	−4.063	0.019	0.095	*Myh1*	−10.133	0.002	0.035
Adra2a	−8.313	0.000	0.017	*Myh9*	−2.359	0.004	0.046
Akap5	−8.506	0.000	0.017	*Myo10*	−4.730	0.006	0.056
Akr7a5	−2.071	0.013	0.081	*Myoc*	−3.234	0.015	0.085
Akt1s1	−2.002	0.004	0.050	*Nat9*	−3.387	0.012	0.078
Anapc5	−2.274	0.001	0.023	*Ndfip1*	−4.237	0.010	0.071
Ankrd13d	−2.118	0.006	0.058	*Ndst3*	−4.583	0.007	0.062
Anp32b	−2.272	0.003	0.040	*Ndufa3*	−2.237	0.017	0.090
Ap1s1	−2.586	0.003	0.040	*Ndufs5*	−2.374	0.018	0.092
Ap2s1	−2.371	0.012	0.078	*Ndufs6*	−3.439	0.000	0.018
Aqr	−2.439	0.019	0.094	*Nes*	−5.213	0.001	0.030
Arhgap26	−3.451	0.000	0.017	*Neurl4*	−2.326	0.005	0.052
Arhgap39	−2.113	0.006	0.058	*Nfkbil1*	−4.943	0.001	0.027
Arhgef11	−2.432	0.016	0.088	*Nfya*	−4.346	0.018	0.093
Ascc2	−10.550	0.001	0.024	*Noct*	−2.815	0.013	0.081
Astn2	−8.207	0.001	0.027	*Nol10*	−2.001	0.001	0.024
Atf6b	−2.528	0.010	0.072	*Nop16*	−2.605	0.001	0.032
Atg2a	−2.559	0.001	0.028	*Nptx1*	−2.018	0.005	0.055
Atm	−2.175	0.017	0.090	*Npy1r*	−3.647	0.007	0.061
Atp2b4	−2.641	0.000	0.017	*Nsun2*	−2.052	0.002	0.037
Atp6v0a1	−3.155	0.001	0.032	*Nts*	−6.880	0.003	0.040
B3gnt8	−2.129	0.015	0.085	*Nuak1*	−2.011	0.003	0.040
Bach1	−4.987	0.002	0.035	*Nup155*	−5.434	0.000	0.021
Baz1b	−2.451	0.016	0.089	*Nup88*	−2.178	0.005	0.050
C130074G19Rik	−6.277	0.001	0.027	*Nyap1*	−2.210	0.003	0.045
Cadm4	−2.525	0.005	0.050	*Obfc1*	−5.064	0.003	0.041
Capn1	−2.714	0.001	0.028	*Obox3*	−3.209	0.002	0.035
Cast	−2.300	0.000	0.017	*Ogfr*	−3.157	0.004	0.047
Ccdc130	−5.043	0.003	0.040	*P2rx3*	−2.594	0.015	0.086
Ccdc3	−2.703	0.021	0.099	*Pabpn1*	−2.231	0.008	0.065
Cct5	−2.433	0.002	0.037	*Palm3*	−2.239	0.010	0.072
Cct7	−2.291	0.004	0.045	*Panx1*	−2.446	0.006	0.056
Cct8	−4.490	0.002	0.034	*Pcbp2*	−5.332	0.003	0.041
Cdc26	−2.164	0.002	0.039	*Pcdh11x*	−7.446	0.000	0.003
Cdh1	−2.230	0.004	0.049	*Pex6*	−2.364	0.005	0.055
Cdk11b	−3.476	0.004	0.047	*Pfdn2*	−2.988	0.004	0.045
Cep85l	−9.647	0.001	0.026	*Pfkp*	−2.031	0.001	0.032
Cetn2	−2.177	0.010	0.072	*Pfn1*	−2.932	0.000	0.020
Ckb	−2.670	0.002	0.035	*Pgls*	−2.444	0.009	0.068
Ckm	−8.225	0.006	0.056	*Phldb2*	−8.699	0.004	0.046
Clgn	−2.261	0.000	0.017	*Pih1d1*	−2.509	0.002	0.035
Clint1	−2.048	0.009	0.067	*Plcb3*	−3.864	0.000	0.018
Clip2	−4.567	0.000	0.015	*Plec*	−3.238	0.000	0.017
Cln6	−3.765	0.001	0.025	*Plekhm1*	−4.182	0.005	0.053
Col1a1	−2.067	0.011	0.074	*Pnpo*	−3.077	0.008	0.066
Col5a2	−7.121	0.021	0.100	*Poll*	−4.050	0.002	0.035
Col5a3	−5.712	0.005	0.050	*Polr2h*	−3.280	0.011	0.075
Col8a1	−7.657	0.002	0.037	*Pop1*	−7.207	0.000	0.001
Cops6	−2.017	0.002	0.037	*Prcc*	−2.257	0.002	0.033
Coq7	−2.086	0.015	0.085	*Prg2*	−10.331	0.000	0.020
Cpe	−2.053	0.002	0.034	*Prkag2*	−2.591	0.000	0.019
Cpt1c	−2.190	0.006	0.059	*Prrx1*	−5.132	0.004	0.047
Cpxm1	−3.325	0.005	0.052	*Psmb3*	−2.915	0.002	0.036

(*Table continues*)

Table 4. Continued

Genes	Log2 fold change	*p*	*q*	Genes	Log2 fold change	*p*	*q*
Csgalnact1	−9.636	0.001	0.028	*Psmb5*	−2.213	0.002	0.036
Csnk2a2	−2.122	0.006	0.059	*Psmc1*	−2.405	0.000	0.016
Csrnp1	−10.669	0.001	0.030	*Psmd13*	−2.670	0.003	0.044
Ctu2	−3.003	0.014	0.084	*Psmd2*	−2.182	0.001	0.027
Cul7	−3.621	0.007	0.062	*Psmd4*	−2.809	0.003	0.044
Cwc25	−2.930	0.004	0.045	*Ptger1*	−3.477	0.018	0.094
Dapk2	−2.224	0.014	0.084	*Ptms*	−3.871	0.002	0.037
Ddx56	−2.158	0.004	0.045	*Ptpn23*	−7.273	0.002	0.036
Dgkz	−2.686	0.003	0.040	*Ptprb*	−7.624	0.000	0.004
Disp1	−2.321	0.015	0.085	*Ptrf*	−4.042	0.005	0.053
Dlg3	−3.824	0.008	0.064	*Pycr2*	−2.066	0.015	0.085
Dnaja2	−2.167	0.001	0.028	*Pygl*	−2.181	0.014	0.083
Dnm1	−2.469	0.009	0.068	*Pygo2*	−2.586	0.007	0.063
Dph2	−6.419	0.000	0.017	*Qsox1*	−2.054	0.003	0.040
Dph7	−6.003	0.000	0.014	*R3hdm4*	−2.054	0.013	0.082
Dpp7	−2.645	0.013	0.080	*Rack1*	−2.006	0.005	0.055
Dpp8	−2.446	0.003	0.042	*Rae1*	−2.346	0.014	0.084
Dpy19l4	−6.024	0.001	0.028	*Rara*	−4.005	0.005	0.053
Dpysl5	−2.386	0.016	0.088	*Rbm14*	−6.125	0.001	0.032
Drg2	−2.986	0.011	0.076	*Rbm6*	−2.191	0.007	0.061
Ebpl	−2.024	0.006	0.056	*Rcc2*	−2.150	0.002	0.037
Edc4	−3.342	0.003	0.040	*Reps1*	−4.535	0.000	0.022
Ehmt2	−2.944	0.008	0.066	*Rexo4*	−3.169	0.015	0.087
Eif2b4	−2.226	0.009	0.068	*Rfc2*	−2.711	0.005	0.054
Eif2b5	−2.424	0.002	0.033	*Riok1*	−2.211	0.017	0.090
Eif3j1	−2.155	0.018	0.092	*Rnf122*	−2.237	0.000	0.018
Eif3m	−2.731	0.006	0.057	*Rnf2*	−2.259	0.015	0.086
Eif5b	−2.048	0.008	0.066	*Rpia*	−2.151	0.017	0.090
Emc1	−2.455	0.004	0.047	*Rpl24*	−3.600	0.003	0.040
Eps8	−7.159	0.003	0.044	*Rplp2*	−2.166	0.003	0.040
Fabp4	−7.365	0.000	0.021	*Rrp1*	−2.684	0.001	0.025
Fam195b	−2.538	0.003	0.043	*Rrp7a*	−2.173	0.010	0.070
Fam21	−2.569	0.001	0.024	*Rsph9*	−3.818	0.009	0.067
Fam65b	−7.543	0.003	0.044	*Rsrc1*	−2.223	0.005	0.054
Fbn1	−5.976	0.004	0.046	*Ryr1*	−9.068	0.021	0.099
Fh1	−2.129	0.006	0.056	*S100a8*	−7.163	0.001	0.025
Fhl3	−3.273	0.014	0.084	*S100a9*	−6.621	0.002	0.033
Fkbp10	−8.824	0.001	0.027	*Sae1*	−2.758	0.008	0.064
Fkbp14	−2.261	0.005	0.053	*Sart3*	−2.174	0.001	0.024
Fnbp4	−4.246	0.012	0.078	*Sass6*	−2.773	0.015	0.087
Frg1	−2.094	0.001	0.030	*Scn2a1*	−4.227	0.008	0.066
Ftsj3	−2.299	0.004	0.048	*Sdad1*	−2.183	0.014	0.084
Gab2	−2.044	0.004	0.047	*Sdk2*	−4.549	0.013	0.081
Gdap1l1	−2.493	0.011	0.074	*Sdsl*	−4.243	0.017	0.092
Gfod2	−2.657	0.010	0.071	*Selenbp1*	−8.748	0.001	0.027
Gga1	−2.391	0.004	0.049	*Senp1*	−5.212	0.018	0.092
Gm21967	−3.888	0.010	0.073	*Sept6*	−2.159	0.006	0.058
Gm42417	−9.870	0.005	0.053	*Serpina11*	−3.644	0.014	0.085
Golga2	−2.272	0.003	0.045	*Sertad1*	−2.157	0.006	0.059
Golga7b	−2.577	0.004	0.047	*Sfrp5*	−2.379	0.001	0.028
Gp1bb	−2.047	0.001	0.030	*Sin3b*	−2.401	0.002	0.032
Gpr179	−8.139	0.001	0.028	*Slc16a3*	−10.302	0.005	0.050
Gpx4	−2.608	0.009	0.069	*Slc25a24*	−8.902	0.000	0.017
Grcc10	−2.915	0.003	0.040	*Slc27a4*	−2.479	0.020	0.097
Gsn	−2.133	0.015	0.085	*Slc39a6*	−2.296	0.002	0.036
Gtf2f2	−9.634	0.003	0.042	*Slc43a1*	−4.289	0.009	0.068
Gys1	−2.353	0.000	0.016	*Slc51a*	−6.814	0.000	0.015
H2afy2	−3.646	0.001	0.026	*Slc7a3*	−2.557	0.018	0.093
Hba-a2	−3.246	0.010	0.072	*Slc7a5*	−3.490	0.000	0.020
Hddc2	−2.355	0.005	0.055	*Slfn2*	−8.252	0.014	0.084
Hdgfrp2	−2.558	0.001	0.028	*Smarcd2*	−3.411	0.018	0.092
Hgf	−3.196	0.008	0.065	*Smarce1*	−2.804	0.016	0.089
Hmgcl	−2.512	0.006	0.058	*Snf8*	−2.088	0.006	0.056
Hnrnpf	−2.067	0.005	0.053	*Snrnp200*	−2.004	0.018	0.093

(*Table continues*)

Table 4. Continued

Genes	Log2 fold change	*p*	*q*	Genes	Log2 fold change	*p*	*q*
Hnrnpk	−2.677	0.000	0.016	*Snw1*	−2.689	0.000	0.016
Hnrnpm	−2.317	0.006	0.057	*Snx9*	−7.202	0.001	0.029
Hoxa10	−7.037	0.000	0.018	*Sox8*	−8.131	0.000	0.012
Hoxa7	−6.596	0.000	0.018	*Sppl3*	−2.328	0.012	0.079
Hoxa9	−6.957	0.000	0.023	*Spred3*	−4.439	0.003	0.040
Hoxb2	−5.943	0.000	0.019	*Srcap*	−3.676	0.007	0.060
Hoxb4	−8.161	0.000	0.017	*Ssb*	−2.140	0.005	0.053
Hoxb5	−7.221	0.000	0.017	*Supt16*	−2.360	0.000	0.018
Hoxb9	−9.174	0.000	0.016	*Syp*	−2.076	0.015	0.087
Hoxc6	−9.853	0.000	0.002	*Taf4b*	−10.301	0.002	0.037
Hoxd10	−7.982	0.001	0.030	*Tango6*	−10.199	0.002	0.037
Hoxd4	−4.810	0.001	0.026	*Tarbp2*	−3.521	0.003	0.040
Hoxd8	−5.752	0.000	0.020	*Tbc1d10b*	−2.056	0.011	0.074
Hoxd9	−7.597	0.005	0.053	*Thap4*	−6.562	0.000	0.017
Hps4	−5.021	0.003	0.042	*Timm50*	−2.701	0.011	0.074
Hsp90ab1	−2.714	0.000	0.018	*Tkt*	−3.256	0.010	0.072
Hspa9	−2.531	0.000	0.023	*Tlx3*	−2.618	0.002	0.035
Ier5l	−5.059	0.006	0.057	*Tmem101*	−2.205	0.015	0.087
Il11ra1	−2.334	0.012	0.078	*Tmem201*	−5.403	0.000	0.020
Ino80	−4.042	0.006	0.057	*Tmem205*	−4.532	0.001	0.026
Irf5	−8.535	0.000	0.004	*Tnnc2*	−9.833	0.001	0.030
Irgq	−2.836	0.010	0.072	*Tnnt3*	−7.545	0.002	0.038
Kdm1a	−2.263	0.006	0.058	*Tnpo2*	−2.492	0.007	0.063
Kdm4b	−8.283	0.010	0.073	*Tnrc18*	−2.271	0.005	0.053
Kif3a	−2.029	0.014	0.084	*Top2a*	−7.193	0.019	0.095
Kif3c	−4.039	0.002	0.035	*Ttbk1*	−2.591	0.007	0.061
Klf2	−6.811	0.001	0.025	*Tubb3*	−2.963	0.000	0.015
Lcmt2	−4.928	0.003	0.040	*Txnrd2*	−2.946	0.008	0.066
Ldlr	−2.419	0.001	0.024	*Ubc*	−2.316	0.002	0.037
Leo1	−2.433	0.008	0.065	*Ube2s*	−2.379	0.009	0.069
Lig1	−2.253	0.002	0.034	*Uchl1*	−3.022	0.009	0.069
Loxl1	−6.618	0.001	0.030	*Uck2*	−2.829	0.006	0.056
Lrrc17	−3.531	0.008	0.064	*Upf3b*	−3.615	0.007	0.060
Lrrfip1	−3.487	0.005	0.050	*Urgcp*	−4.220	0.001	0.029
Lta4 h	−2.258	0.003	0.042	*Usp17la*	−7.689	0.000	0.016
Ltbp3	−2.457	0.007	0.062	*Utp18*	−4.338	0.009	0.068
Man2b2	−8.690	0.000	0.018	*Vezt*	−2.143	0.015	0.087
Map1a	−2.487	0.002	0.035	*Vps33a*	−2.623	0.008	0.066
Mb	−9.449	0.002	0.035	*Vps8*	−3.249	0.000	0.018
Mboat1	−5.624	0.003	0.041	*Xirp2*	−8.750	0.002	0.038
Mcoln1	−2.973	0.012	0.079	*Yipf1*	−2.497	0.001	0.025
Mdfic	−10.177	0.001	0.032	*Zfp212*	−2.281	0.013	0.081
Med16	−2.428	0.018	0.092	*Zfp292*	−2.238	0.015	0.086
Med29	−2.799	0.008	0.064	*Zfp30*	−6.842	0.002	0.035
Mfap4	−4.773	0.003	0.045	*Zfp384*	−4.615	0.004	0.049
Mgat4c	−5.486	0.002	0.035	*Zfp428*	−2.044	0.003	0.045

Next, we evaluated correlation between differentially transcribed and translated mRNAs between the TG and DRG. To do this, we plotted the 379 mRNAs with higher transcript levels in TG and 315 with higher levels in the DRG. We plotted these against TPMs from the Nav1.8-TRAP datasets from both tissues. We did the same thing for the 372 Nav1.8-TRAP enriched mRNAs from TG and 348 from DRG and compared these with TPMs from input RNA sequencing (Fig. 4*C*). We observed that only 144 genes were shared between these datasets, suggesting that transcriptional and translational regulation is decoupled in these tissues, at least for the most highly enriched genes. This finding is consistent with genome-wide experiments showing that transcription and translation are decoupled for many, if not most, mRNAs (Liu et al., 2016).

We then sought to validate some specific findings from whole transcriptome or Nav1.8-TRAP sequencing data obtained from

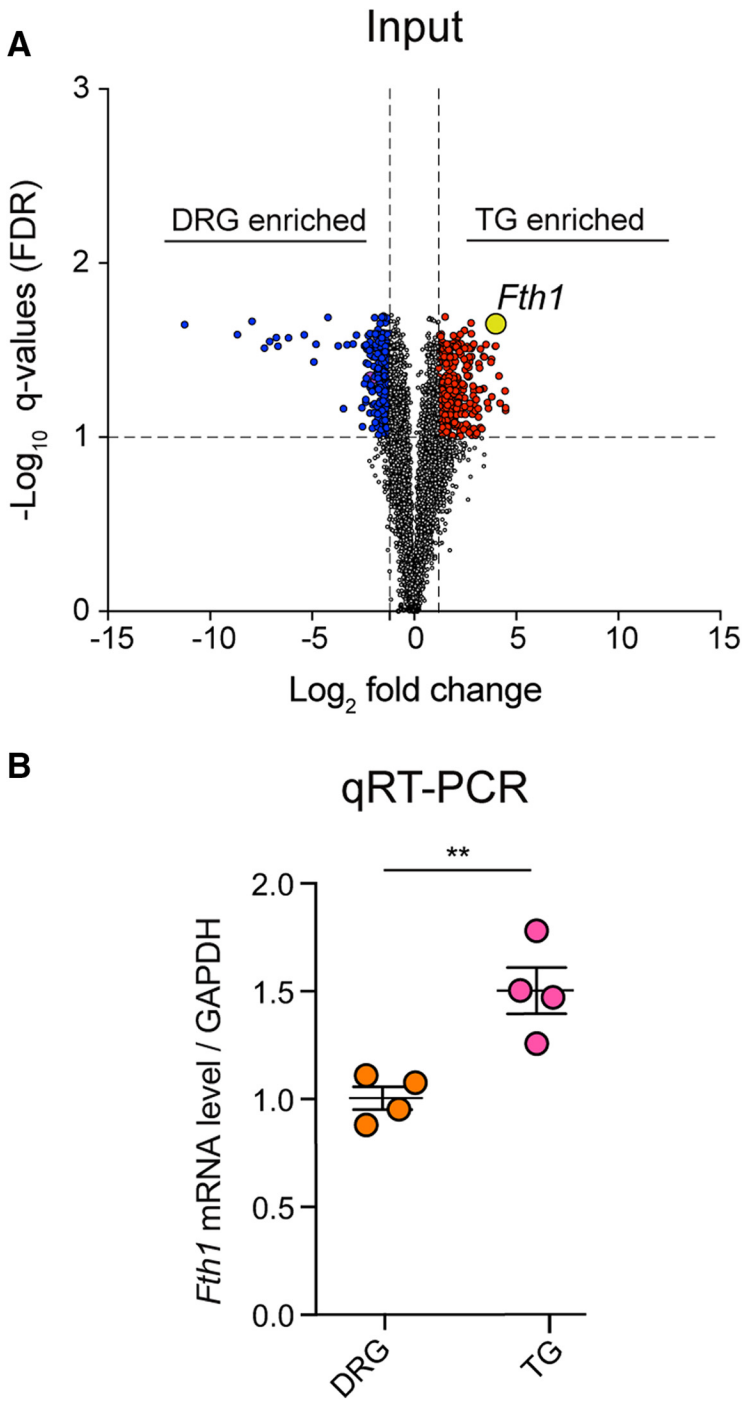

Figure 5. RNA-seq analysis reveals *Fth1* as differentially expressed in the TG and validated through qRT-PCR. ***A***, Volcano plot shows *Fth1* (yellow dot) as being significantly enriched in TG versus DRGs. ***B***, qRT-PCR shows a 50% increase in *Fth1* mRNA expression in TG. (paired *t* test, $t = 4{,}15$; df $= 6$; $^{**}p = 0.0048$).

the comparison between TG and DRG. Analysis of the differentially expressed genes between TG and DRG showed that *Fth1* is highly enriched in the TG (Fig. 5*A*). We used qRT-PCR on mRNA prepared from both tissues to validate that there is a significant enrichment of *Fth1* mRNA in the TG by this method (Fig. 5*B*). Comparisons of the TG and DRG transcriptome showed that multiple genes among the AMPK pathway were enriched in the DRG, such as *Prkag2*, *Acacb*, *Akt1s1*, and *Gys* (Fig. 6*A*). Interestingly, these same mRNAs were among the 144 that were regulated at the translational level as well (Fig. 6*A*), but there were also a number of additional mRNAs involved in the AMPK pathway that were only found in the translatome dataset, including *Cpt1c* and *Acaca*. In stark contrast, we observed an enrichment of mRNAs in the translatome in the TG that are associated with the PI3K-mTORC1 pathway, including *Strada*, *Lamtor5*, *Akt1*, and *Rraga* (Fig. 6*A*, *B*). As mentioned previously, this predicts a higher level of mTOR activity in TG than in the DRG nociceptors. To begin to address this prediction, we examined steady-state protein levels for selected targets between DRG and TG. We chose to focus on *RragA*, which encodes the RagA protein, because it is a critical activator of mTORC1 activity that links mTORC1 to amino acid and glucose signaling at the interface with lysosomes (Efeyan et al., 2013, 2014). Consistent with transcriptome data, we observed no differences in the level of *Rraga* mRNA between TG and DRG, but we did detect a significant increase in protein level in the TG versus the DRG (Fig. 6*C*). We have previously shown that *Rraga* mRNA translation is finely controlled by the activity of Mnk1 and correlated with the level of eIF4E phosphorylation. Here, we also detected a higher level of eIF4E phosphorylation in the TG compared with DRG (Fig. 6*D*), suggesting that TG nociceptors may display higher translational activity via this pathway than their DRG counterparts (Megat et al., 2019). We also focused on *Akt1s1*, which encodes the PRAS40 protein, because this is a negative regulator of mTORC1 activity with actions that are inversely related to RagA (Wiza et al., 2012; Chong, 2016). In the DRG, we observed that the level of the ribosome-associated *Akt1s1* mRNAs was higher in the DRG compared with TG, and this was validated by increased PRAS40 protein in DRG (Fig. 6*E*).

Collectively, the results described above suggest that the balance of mTORC1 signaling through the lysosome is shifted toward activation in the TG compared with the DRG, which could influence nociceptive responses in the facial area compared with areas innervated by the DRG. To test this hypothesis, we gave injections of a low dose of capsaicin (0.1 μM), a TRPV1 agonist, into the hindpaw and the whisker pad (facial area). We observed a significantly more pronounced spontaneous pain response following facial capsaicin compared with the hindpaw (Fig. 6*F*). Also, the intensity/number of the nocifensive behavior was significantly larger following injection of capsaicin into the cheek, again suggesting that nociceptive stimuli trigger larger behavioral responses when administered in the facial area (Fig. 6*F*). We next sought to investigate whether capsaicin-induced nocifensive behavior was dependent on

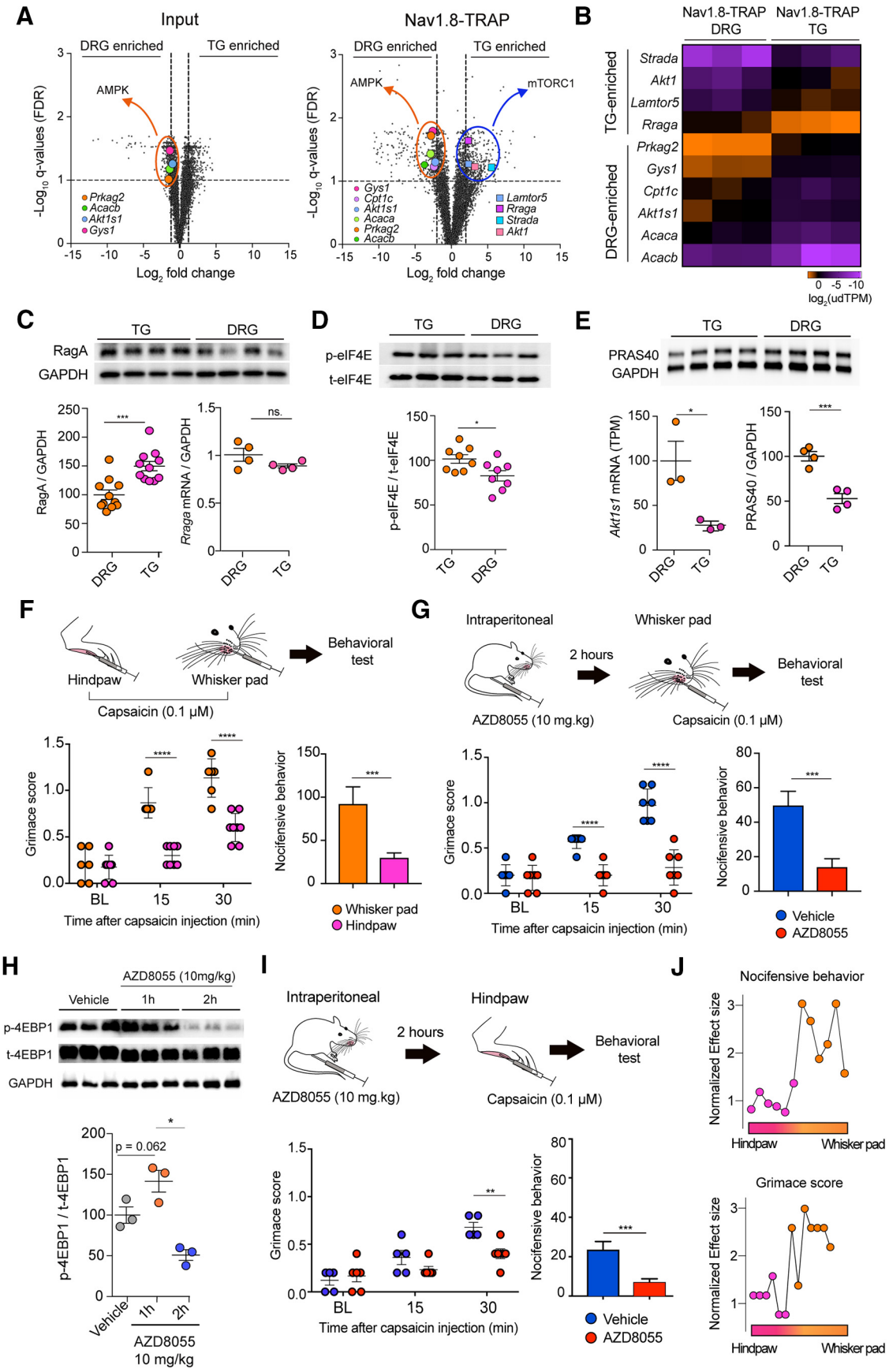

Figure 6. TRAP-seq analysis reveals that AMPK- and mTORC1-related genes are differential expressed and/or translated in the DRG and TG, respectively. ***A***, Volcano plot showing an enrichment in AMPK-related genes in the input DRG sample, including *Prkag2*, *Akt1s1*, *Gys1*, *Acacb*, as well as in TRAP-seq (including *Prkag2*, *Akt1s1*, *Gys1*, *Acacb*, *Acaca*, and *Cpt1c*). In converse, mTORC1-related genes are enriched in TG, such as *Strada*, *Rraga*, *Akt*, and *Lamtor5*. ***B***, Heatmap shows increase translation of AMPK and mTORC1 genes in the DRGs and TG, respectively. (*Figure legend continues.*)

mTORC1 activity in the TG region. We treated animals with an mTORC1 inhibitor (AZD8055, 10 mg/kg) 2 h before injection of capsaicin into the whisker pad. We observed that the mTORC1 inhibitor significantly attenuated grimace responses and nocifensive behaviors (Fig. 6*G*), and this behavioral change correlated with a significant decrease in the level of p-4EBP1 (Fig. 6*H*), a downstream target of mTORC1. While we also observed that mTORC1 inhibition significantly attenuated grimace responses and nocifensive behavior induced by a plantar injection of capsaicin (Fig. 6*I*), the effect size was significantly smaller compared with capsaicin into the whisker pad (Fig. 6*J*). Previous clinical findings reported that repetitive noxious heat stimulation, which also acts via TRPV1, creates greater sensitization in the TG region in people (Schmidt et al., 2015). Our findings parallel these observations and support a model wherein enhanced mTORC1 signaling in TG nociceptors is a cause of this enhanced sensitization.

Combining the datasets described above with single-cell RNA sequencing from existing data sources (Usoskin et al., 2015; Hu et al., 2016) allowed us to infer translation efficiencies (TEs) for all mRNAs translated in Nav1.8 neurons. First, we used the most discriminative genes in each cell type cluster (Hu et al., 2016) and calculated the correlation coefficients with all the protein coding genes in our Nav.8-TRAP sequencing datasets. Then, we plotted the heatmap of the correlation coefficient, and we observed a clear cluster of genes highly correlated with *Scn10a* (Fig. 7*A*). The *Scn10a* cluster (2594 genes) was compared with our TRAP-filtered dataset (7358 genes), which generated a list of 854 *Scn10a*-enriched genes (Fig. 7*A*). We then looked at the expression level of the *Scn10a*-enriched genes and calculated the TEs (the ratio of the TRAP and Input values) for each gene in TG and DRG datasets. Cluster 1 (C1) identified the *Scn10a*-enriched genes showing high TEs in the DRG (Fig. 7*B*; Fig. 7-1, available at https://doi.org/10.1523/JNEUROSCI.2663-18.2019.f7-1). Among them, we again found *Acaca* that codes for the protein ACC (acetyl-CoA carboxylase 1), a downstream target of AMPK (Hardie, 2014). Cluster 2 (C2) identified genes showing high TEs in the TG, such as *Lamtor5*, *Rraga*, and *Fkbp1a*, all important regulators of the mTORC1 pathway (Fig. 7*B*; Fig. 7-1, available at https://doi.org/10.1523/JNEUROSCI.2663-18.2019.f7-1). This cluster also identified the CGRPβ mRNA *Calcb* and the MrgprD receptor mRNA. Cluster (C3) contained genes with low TEs in both TG and DRG, and cluster 4 (C4) identifies genes with high TE in TG and DRG (Fig. 7-1, available at https://doi.org/10.1523/JNEUROSCI.2663-18.2019.f7-1). Finally, we examined functional gene families (e.g., ion channels, GPCRs and kinases) for any systematic differences in TEs for mRNAs expressed in Nav1.8$^+$ nociceptors in the TG. Interestingly, we observed that ion channels and GPCRs tend to show higher TEs compared with other gene families, such as kinases or transcription factors (Fig. 7*C*; Fig. 7-2, available at https://doi.org/10.1523/JNEUROSCI.2663-18.2019.f7-2), a finding that is consistent with observations in DRG Nav1.8-expressing neurons (Megat et al., 2019).

Finally, we used MEME Suite (Bailey et al., 2015) to search for motifs in the 5′ UTRs of mRNAs in clusters 1–4 described above. We only considered motifs that were found in >30% of genes in each of the clusters. In C1, we did not identify any enriched motifs; however, in C2, we identified 2 motifs in mRNAs of 5′-UTRs for genes with increased TE in the TG versus the DRG (Fig. 8). One of these was a GC-rich motif found in 82 of 307 mRNAs, and another was a terminal oligo pyrimidine tract motif found in 57 of 307 mRNAs. The latter motif is interesting because it is consistent with the finding that mTORC1 genes are more translated in the TG because terminal oligo pyrimidine tract element containing mRNAs show increased TE when mTORC1 activity is high (Thoreen et al., 2012). In the C3 cluster, which contains mRNAs with low TEs in both TG and DRG, we found a G quadruplex motif (57 of 193 mRNAs) (Fig. 8) that is likely a target for eIF4A-mediated translation control (Wolfe et al., 2014), suggesting that eIF4A activity might be low under normal conditions in TG and DRG neurons. We did not find any enriched motifs in C4.

Discussion

Our work uses the TRAP technology to highlight differences in the translatomes of Nav1.8$^+$ neurons in the DRG and TG. Although there are many consistencies between these tissues, as would be expected by the similar function of Nav1.8$^+$ neurons in the DRG and TG, there are some striking differences that may have important functional implications. Prominent among these are higher levels of protein synthesis for many regulators of the mTORC1 pathway in the TG and higher protein synthesis for members of the AMPK signaling pathway in the DRG. mTORC1 is a well-known downstream target of the AMPK kinase (Alers et al., 2012). It has been documented that, under energy-low conditions, increases in AMPK activity inhibit mTORC1, resulting in decreased overall protein synthesis and promotion of autophagy mechanisms (Schmidt et al., 2016). Because these signaling pathways regulate one another, this suggests that mRNAs that are regulated by the mTORC1 pathway are likely to have higher translational efficiencies in the TG than in the DRG. Previous psychophysical studies in humans have shown that painful stimulation of the TG area causes greater sensitization than stimulation of DRG-innervated regions (Schmidt et al., 2015, 2016). These studies have also demonstrated a lack of habitation in the TG region with repeated painful thermal stimulation (Schmidt et al., 2015). It is now well established that the mTORC1 signaling pathway plays a key role in controlling nociceptor excitability and sensitization (Melemedjian et al., 2010; Moy et al., 2017; Khou-

←

(*Figure legend continued.*) ***C***, Immunoblotting shows an upregulation of RagA protein inTG (RagA: DRG = 100 ± 8.39,T = 149.8 ± 8.03, $*p = 0.0003$, $n = 11$), whereas *Rraga* mRNA measured by qRT-PCR was not different between DRGs and TG (*Rraga*: DRG = 1.120 ± 0.075, TG = 1.01 ± 0.024, $p = 0.152$, $n = 4$). ***D***, Immunoblotting shows a lower level of eIF4E phosphorylation in the DRG compared with TG (p-eIF4E: TG = 100.5 ± 4.28, DRG = 79.98 ± 7.13, $*p = 0.0404$). ***E***, The negative regulator of mTORC1, PRAS40 (*Akt1s1*) mRNA, and TE was significantly increased in DRGs and confirmed by an increase in protein level (Akt1s1: DRG = 100 ± 5.28, TG = 52.62 ± 5.48, $***p = 0.008$, $n = 4$). ***F***, Nocifensive behavior and grimace score after injection of capsaicin (0.1 μM) into the whisker pad or the hindpaw. Capsaicin induces a more intense affective response when injected into the whisker pad compared with the hindpaw as shown by the mouse grimace score at 15 and 30 min (two-way ANOVA: $F_{(2,24)} = 22.98$, $****p < 0.0001$, *post hoc* Sidak $****p < 0.0001$ at 15 and 30 min). Likewise, nocifensive behavior is more pronounced when capsaicin was injected into the whisker pad compared with the hindpaw ($F_{(1,12)} = 11.62$, $**p < 0.0052$, *post hoc* Sidak $***p = 0.002$ at 60 min after capsaicin). ***G***, Pretreatment with an mTORC1 inhibitor (AZD8055, 10 mg/kg) blocked capsaicin-induced nocifensive behavior in the whisker pad ($F_{(2,24)} = 13.93$, $****p < 0.0001$, *post hoc* Sidak $***p = 0.002$ at 60 min after capsaicin) and affective pain ($F_{(2,24)} = 21.62$, $****p < 0.0001$, *post hoc* Sidak $****p < 0.0001$ at 15 and 30 min). ***H***, Intraperitoneal injection of AZD8055 (10 mg/kg) decreased the level of p-4EBP1 at 2 h (one-way ANOVA: $F_{(2,6)} = 19.15$, $**p = 0.0025$, *post hoc* Dunnett: Veh vs 2 h, $*p = 0.027$) in the TG. ***I***, AZD8055 inhibited capsaicin-induced grimace at 30 min ($F_{(2,27)} = 4.52$, $*p = 0.02$, *post hoc* Sidak $**p = 0.0034$) and nocifensive behavior ($F_{(1,9)} = 17.45$, $**p < 0.0024$, *post hoc* Sidak $***p < 0.001$ at 60 min after capsaicin) when injected into the hindpaw. ***J***, For each group of animals, the difference between the vehicle- and AZD8055-treated values was calculated and plotted for the nocifensive behavior and mouse grimace score. We observed a significantly larger effect size of AZD8055 in nocifensive behavior (unpaired *t* test, $t = 3.52$, df = 11, $**p = 0.0048$) and grimacing (unpaired *t* test, $t = 5.54$, df = 11, $***p = 0.0002$) when capsaicin was injected in the whisker pad. ns, not significant.

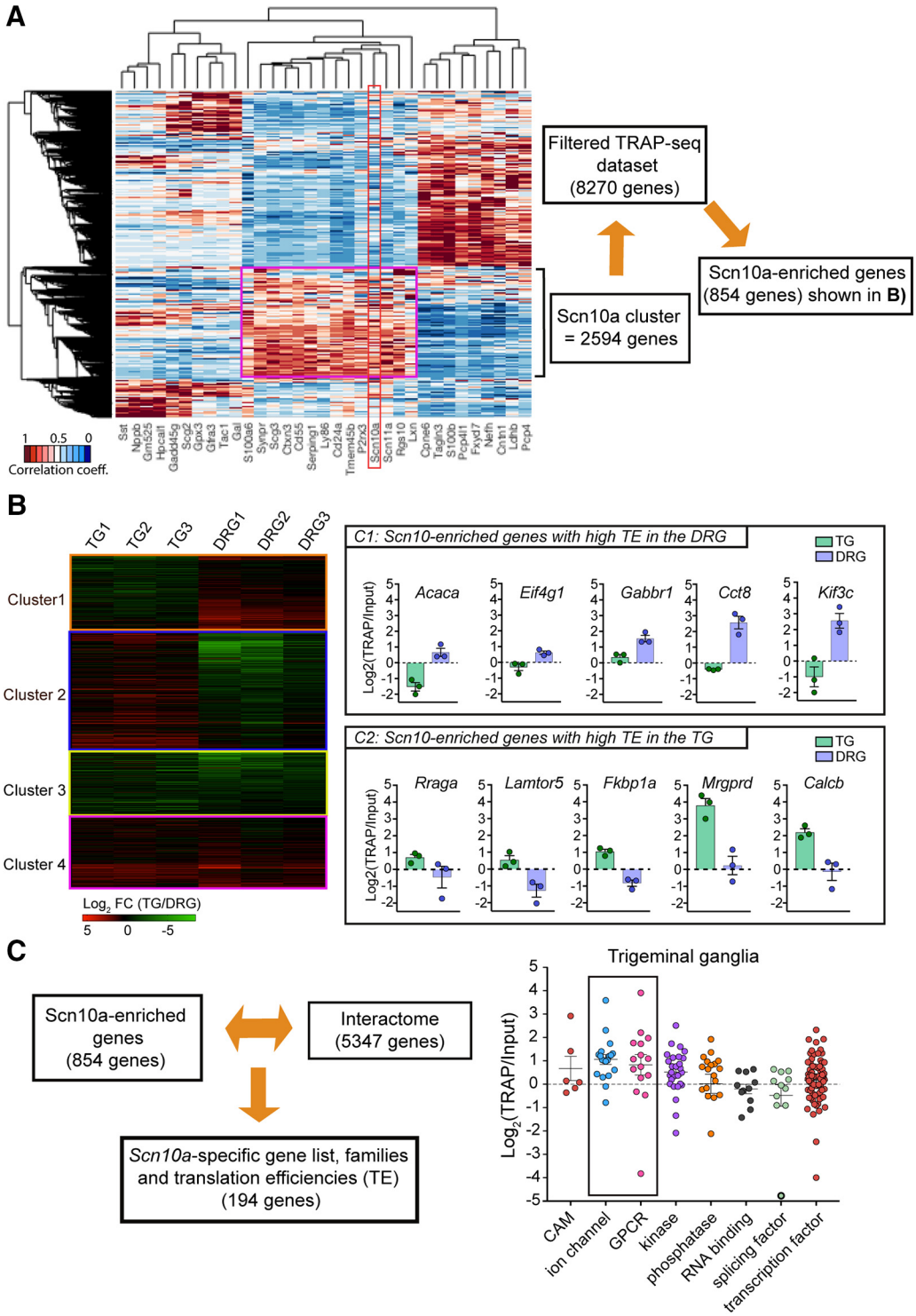

Figure 7. TE analysis for Scn10a-enriched genes in TG- and DRG-TRAP-seq shows differential TEs between tissues. ***A***, Heatmap showing the correlation coefficient of the protein coding genes with the most discriminative expression between cell populations based on the DRG single-cell dataset published previously (Usoskin et al., 2015; Hu et al., 2016) with Nav1.8 (*Scn10a*) highlighted. A cluster of 2547 genes was identified as highly enriched in the *Scn10a*-positive neuronal population. Those 2547 genes were then merged to the TRAP-seq filtered dataset (~8000 genes) to identify a group of 854 mRNAs that were highly enriched in the single-cell population that also expressed *Scn10a* and not found in other cell populations. ***B***, Heatmap of the TE for the 854 mRNAs shows 4 separate clusters. C1 identifies mRNAs with high TEs in the DRG but lower in TG. C2 shows genes with high TE in the TG and low TEs in the DRG. C3 identifies mRNAs with low TEs in both tissues. C4 identifies mRNAs with high TEs in both tissues. ***C***, Calculation of TE efficiencies for gene families in the TG shows higher TEs for mRNAs coding for ion channels and GPCRs compared with splicing and transcription factors. Figure 7-1 (available at https://doi.org/10.1523/JNEUROSCI.2663-18.2019.f7-1) shows estimated TEs for all genes shown in clusters in Figure 7*A*. Figure 7-2 (available at https://doi.org/10.1523/JNEUROSCI.2663-18.2019.f7-2) shows estimated TEs by gene family.

torsky and Price, 2018), and this sensitization is strongly attenuated by activation of the AMPK pathway (Melemedjian et al., 2011; Burton et al., 2017). Our findings are in line with somatotopic differences in response to painful stimulation and a higher propensity to sensitization in TG nociceptors. While this might be explained by the biological relevance of the head and facial area for vital functions, our data show that differences in basal mTORC1 activity between TG and DRG nociceptors could drive

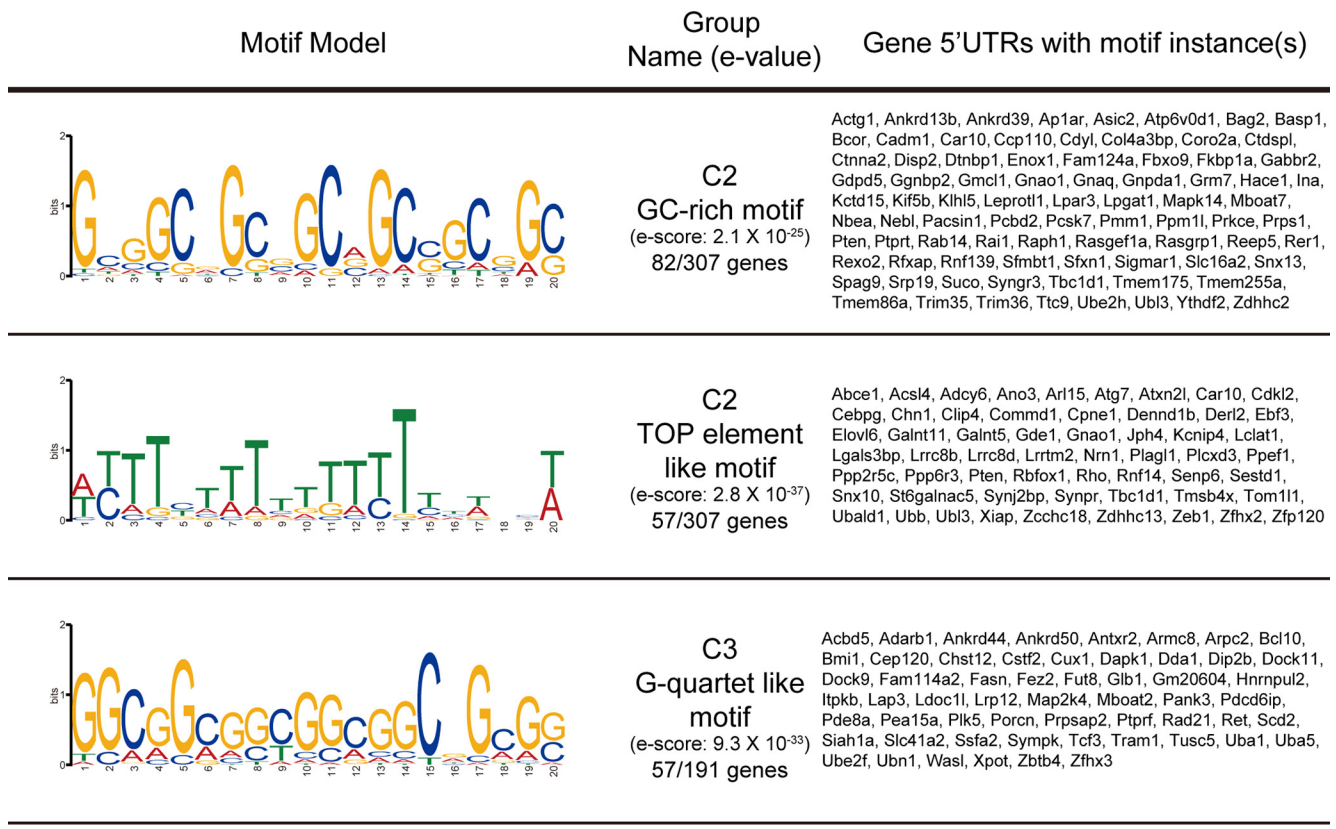

Figure 8. mRNA motifs enriched in 5′-UTRs from clusters of genes that show altered TEs between TG and DRG. Two motifs were found in cluster C2 (higher TE in TG than in DRG) and 1 motif was found in cluster C3 (low TE in both TG and DRG). Genes with motifs found in their 5′-UTRs are shown to the right of the corresponding motifs.

differences in magnitude of sensitization following injury. However, it is also important to note that recently discovered anatomical differences between central projections of DRG and TG neurons may also mediate these differences (Rodriguez et al., 2017), in particular as they relate to enhanced fear and anxiety from painful stimulation of the TG region (Schmidt et al., 2016).

A recent paper examined differences in mRNA expression on FACS-sorted TG and DRG neurons from mice, demonstrating that >99% of mRNA showed consistent expression between TG and DRG neurons (Lopes et al., 2017). These authors only identified 24 mRNAs with differential expression, but these included Hox genes, as we also found, and an arginine vasopressin receptor (Lopes et al., 2017). Many other differentially expressed genes they attributed to non-neuronal cell types. We found >300 differentially expressed genes in the whole tissue transcriptome of the DRG versus the TG, and many of these mRNAs may be attributable to non-neuronal cells because we did not sort cells for whole transcriptome. This likely explains the major discrepancies between transcriptomes in these two papers. However, major differences in translatome findings cannot be attributable to non-neuronal cells because the approach we use is specific to Nav1.8-expressing neurons, most of which are nociceptors. Our work also identifies potential differences in translation regulation signaling between the DRG and TG that provides a plausible explanation for these difference in the translatome. This is especially important considering that the mTOR (Patursky-Polischuk et al., 2009; Thoreen et al., 2012) and AMPK (Dowling et al., 2007) pathways have distinct effects on TE of specific subsets of mRNAs.

There are limitations to our approach. Primary among these is that our TE estimates could only be applied to a subset of genes that have been identified as highly enriched in the Nav1.8$^+$ population of neurons by single-cell RNA sequencing. Future efforts may use cell-sorting techniques (Thakur et al., 2014; Lopes et al., 2017) for transcriptome generation in combination with TRAP sequencing to make estimates of the TE across the active genome of Nav1.8$^+$ population of cells. A technical shortcoming of this potential approach is that tissue homogenization and cellular dissociation protocols that are needed to sort cells for transcriptomic analysis cause induction of classes of genes, including molecular chaperones and immediate early genes that can bias transcriptomes and distort TE estimates (van den Brink et al., 2017). A second limitation is that, while our data are suggestive of important differences in mTORC1 and AMPK signaling between these two tissues that may regulate susceptibility to nociceptor sensitization, we have not shown this directly with behavioral or electrophysiological evidence. However, the notion of that TG nociceptors are more intensely sensitized by noxious stimuli is supported by preclinical models and human psychophysical data (Schmidt et al., 2015, 2016). For example, it has recently been demonstrated that injury to TG nerves induces a grimacing effect in both rats and mice (Akintola et al., 2017). This is in stark contrast to effects of injury to the sciatic nerve where grimacing effects are not observed (Langford et al., 2010). These findings suggest that injury to TG nerves induces a stronger ongoing pain phenotype in both of these rodent species. Additional work is needed to clarify whether this is driven by the mTOR signaling axis in the TG.

The results presented here add to a growing body of literature that there are important differences between the DRG and TG that are likely relevant for understanding pain disorders that originate from these regions. These include differential developmen-

tal origins (Zou et al., 2004), differential expression of neuronal subtype markers (Price and Flores, 2007), and altered response to injury, such as sympathetic sprouting into the DRG in response to injury (Chung et al., 1996; Chien et al., 2005; Xie et al., 2007, 2015), which does not occur in the TG (Bongenhielm et al., 1999). Our use of the TRAP technique to define the translatomes of Nav1.8$^+$ neurons in DRG and TG points to a host of newly discovered differences between these two tissues and generates a new resource that can be mined to gain addition insight.

References

Akintola T, Raver C, Studlack P, Uddin O, Masri R, Keller A (2017) The grimace scale reliably assesses chronic pain in a rodent model of trigeminal neuropathic pain. Neurobiol Pain 2:13–17.

Alers S, Loffler AS, Wesselborg S, Stork B (2012) Role of AMPK-mTOR-Ulk1/2 in the regulation of autophagy: cross talk, shortcuts, and feedbacks. Mol Cell Biol 32:2–11.

Bailey TL, Johnson J, Grant CE, Noble WS (2015) The MEME Suite. Nucleic Acids Res 43:W39–W49.

Bongenhielm U, Boissonade FM, Westermark A, Robinson PP, Fried K (1999) Sympathetic nerve sprouting fails to occur in the trigeminal ganglion after peripheral nerve injury in the rat. Pain 82:283–288.

Burton MD, Tillu DV, Mazhar K, Mejia GL, Asiedu MN, Inyang K, Hughes T, Lian B, Dussor G, Price TJ (2017) Pharmacological activation of AMPK inhibits incision-evoked mechanical hypersensitivity and the development of hyperalgesic priming in mice. Neuroscience 359:119–129.

Chien SQ, Li C, Li H, Xie W, Pablo CS, Zhang JM (2005) Sympathetic fiber sprouting in chronically compressed dorsal root ganglia without peripheral axotomy. J Neuropathic Pain Symptom Palliation 1:19–23.

Chong ZZ (2016) Targeting PRAS40 for multiple diseases. Drug Discov Today 21:1222–1231.

Chung K, Lee BH, Yoon YW, Chung JM (1996) Sympathetic sprouting in the dorsal root ganglia of the injured peripheral nerve in a rat neuropathic pain model. J Comp Neurol 376:241–252.

Devor M (1999) Unexplained peculiarities of the dorsal root ganglion. Pain Suppl 6:S27–S35.

Dowling RJ, Zakikhani M, Fantus IG, Pollak M, Sonenberg N (2007) Metformin inhibits mammalian target of rapamycin-dependent translation initiation in breast cancer cells. Cancer Res 67:10804–10812.

Doyle JP, Dougherty JD, Heiman M, Schmidt EF, Stevens TR, Ma G, Bupp S, Shrestha P, Shah RD, Doughty ML, Gong S, Greengard P, Heintz N (2008) Application of a translational profiling approach for the comparative analysis of CNS cell types. Cell 135:749–762.

Dubin AE, Patapoutian A (2010) Nociceptors: the sensors of the pain pathway. J Clin Invest 120:3760–3772.

Durham PL, Garrett FG (2010) Development of functional units within trigeminal ganglia correlates with increased expression of proteins involved in neuron-glia interactions. Neuron Glia Biol 6:171–181.

Efeyan A, Zoncu R, Chang S, Gumper I, Snitkin H, Wolfson RL, Kirak O, Sabatini DD, Sabatini DM (2013) Regulation of mTORC1 by the rag GTPases is necessary for neonatal autophagy and survival. Nature 493:679–683.

Efeyan A, Schweitzer LD, Bilate AM, Chang S, Kirak O, Lamming DW, Sabatini DM (2014) RagA, but not RagB, is essential for embryonic development and adult mice. Dev Cell 29:321–329.

Flegel C, Schöbel N, Altmüller J, Becker C, Tannapfel A, Hatt H, Gisselmann G (2015) RNA-Seq analysis of human trigeminal and dorsal root ganglia with a focus on chemoreceptors. PLoS One 10:e0128951.

Fortelny N, Overall CM, Pavlidis P, Freue GV (2017) Can we predict protein from mRNA levels? Nature 547:E19–E20.

Glusman G, Caballero J, Robinson M, Kutlu B, Hood L (2013) Optimal scaling of digital transcriptomes. PLoS One 8:e77885.

Gong L, Wu J, Zhou S, Wang Y, Qin J, Yu B, Gu X, Yao C (2016) Global analysis of transcriptome in dorsal root ganglia following peripheral nerve injury in rats. Biochem Biophys Res Commun 478:206–212.

Hardie DG (2014) AMPK-sensing energy while talking to other signaling pathways. Cell Metab 20:939–952.

Hardie DG (2015) AMPK: positive and negative regulation, and its role in whole-body energy homeostasis. Curr Opin Cell Biol 33:1–7.

Heiman M, Schaefer A, Gong S, Peterson JD, Day M, Ramsey KE, Suárez-Fariñas M, Schwarz C, Stephan DA, Surmeier DJ, Greengard P, Heintz N (2008) A translational profiling approach for the molecular characterization of CNS cell types. Cell 135:738–748.

Heiman M, Kulicke R, Fenster RJ, Greengard P, Heintz N (2014) Cell type-specific mRNA purification by translating ribosome affinity purification (TRAP). Nat Protoc 9:1282–1291.

Hu G, Huang K, Hu Y, Du G, Xue Z, Zhu X, Fan G (2016) Single-cell RNA-seq reveals distinct injury responses in different types of DRG sensory neurons. Sci Rep 6:31851.

Ingolia NT (2016) Ribosome footprint profiling of translation throughout the genome. Cell 165:22–33.

Isensee J, Wenzel C, Buschow R, Weissmann R, Kuss AW, Hucho T (2014) Subgroup-elimination transcriptomics identifies signaling proteins that define subclasses of TRPV1-positive neurons and a novel paracrine circuit. PLoS One 9:e115731.

Kammermeier L, Reichert H (2001) Common developmental genetic mechanisms for patterning invertebrate and vertebrate brains. Brain Res Bull 55:675–682.

Khoutorsky A, Price TJ (2018) Translational control mechanisms in persistent pain. Trends Neurosci 41:100–114.

Kogelman LJ, Christensen RE, Pedersen SH, Bertalan M, Hansen TF, Jansen-Olesen I, Olesen J (2017) Whole transcriptome expression of trigeminal ganglia compared with dorsal root ganglia in rattus norvegicus. Neuroscience 350:169–179.

Kuleshov MV, Jones MR, Rouillard AD, Fernandez NF, Duan Q, Wang Z, Koplev S, Jenkins SL, Jagodnik KM, Lachmann A, McDermott MG, Monteiro CD, Gundersen GW, Ma'ayan A (2016) Enrichr: a comprehensive gene set enrichment analysis web server 2016 update. Nucleic Acids Res 44:W90–W97.

Langford DJ, Bailey AL, Chanda ML, Clarke SE, Drummond TE, Echols S, Glick S, Ingrao J, Klassen-Ross T, Lacroix-Fralish ML, Matsumiya L, Sorge RE, Sotocinal SG, Tabaka JM, Wong D, van den Maagdenberg AM, Ferrari MD, Craig KD, Mogil JS (2010) Coding of facial expressions of pain in the laboratory mouse. Nat Methods 7:447–449.

Liu Y, Beyer A, Aebersold R (2016) On the dependency of cellular protein levels on mRNA abundance. Cell 165:535–550.

Lopes DM, Denk F, McMahon SB (2017) The molecular fingerprint of dorsal root and trigeminal ganglion neurons. Front Mol Neurosci 10:304.

Manteniotis S, Lehmann R, Flegel C, Vogel F, Hofreuter A, Schreiner BS, Altmüller J, Becker C, Schöbel N, Hatt H, Gisselmann G (2013) Comprehensive RNA-seq expression analysis of sensory ganglia with a focus on ion channels and GPCRs in trigeminal ganglia. PLoS One 8:e79523.

Megat S, Ray PR, Moy JK, Lou TF, Barragán-Iglesias P, Li Y, Pradhan G, Wanghzou A, Ahmad A, Burton MD, North RY, Dougherty PM, Khoutorsky A, Sonenberg N, Webster KR, Dussor G, Campbell ZT, Price TJ (2019) Nociceptor translational profiling reveals the RagA-mTORC1 network as a critical generator of neuropathic pain. J Neurosci 39:393–411.

Melemedjian OK, Asiedu MN,Tillu DV, Sanoja R, Yan J, Lark A, Khoutorsky A, Johnson J, Peebles KA, Lepow T, Sonenberg N, Dussor G, Price TJ (2011) Targeting adenosine monophosphate-activated protein kinase (AMPK) in preclinical models reveals a potential mechanism for the treatment of neuropathic pain. Mol Pain 7:70.

Melemedjian OK, Asiedu MN, Tillu DV, Peebles KA, Yan J, Ertz N, Dussor GO, Price TJ (2010) IL-6- and NGF-induced rapid control of protein synthesis and nociceptive plasticity via convergent signaling to the eIF4F complex. J Neurosci 30:15113–15123.

Moy JK, Khoutorsky A, Asiedu MN, Black BJ, Kuhn JL, Barragán-Iglesias P, Megat S, Burton MD, Burgos-Vega CC, Melemedjian OK, Boitano S, Vagner J, Gkogkas CG, Pancrazio JJ, Mogil JS, Dussor G, Sonenberg N, Price TJ (2017) The MNK-eIF4E signaling axis contributes to injury-induced nociceptive plasticity and the development of chronic pain. J Neurosci 37:7481–7499.

Patursky-Polischuk I, Stolovich-Rain M, Hausner-Hanochi M, Kasir J, Cybulski N, Avruch J, Rüegg MA, Hall MN, Meyuhas O (2009) The TSC-mTOR pathway mediates translational activation of TOP mRNAs by insulin largely in a raptor- or rictor-independent manner. Mol Cell Biol 29:640–649.

Price TJ, Flores CM (2007) Critical evaluation of the colocalization between calcitonin gene-related peptide, substance P, transient receptor potential vanilloid subfamily type 1 immunoreactivities, and isolectin B4 binding in primary afferent neurons of the rat and mouse. J Pain 8:263–272.

Reynders A, Mantilleri A, Malapert P, Rialle S, Nidelet S, Laffray S, Beurrier C,

Bourinet E, Moqrich A (2015) Transcriptional profiling of cutaneous MRGPRD free nerve endings and C-LTMRs. Cell Rep 10:1007–1019.

Rodriguez E, Sakurai K, Xu J, Chen Y, Toda K, Zhao S, Han BX, Ryu D, Yin H, Liedtke W, Wang F (2017) A craniofacial-specific monosynaptic circuit enables heightened affective pain. Nat Neurosci 20:1734–1743.

Schmidt K, Schunke O, Forkmann K, Bingel U (2015) Enhanced short-term sensitization of facial compared with limb heat pain. J Pain 16:781–790.

Schmidt K, Forkmann K, Sinke C, Gratz M, Bitz A, Bingel U (2016) The differential effect of trigeminal vs. peripheral pain stimulation on visual processing and memory encoding is influenced by pain-related fear. Neuroimage 134:386–395.

Stirling LC, Forlani G, Baker MD, Wood JN, Matthews EA, Dickenson AH, Nassar MA (2005) Nociceptor-specific gene deletion using heterozygous NaV1.8-cre recombinase mice. Pain 113:27–36.

Takeda M, Takahashi M, Matsumoto S (2008) Contribution of activated interleukin receptors in trigeminal ganglion neurons to hyperalgesia via satellite glial interleukin-1beta paracrine mechanism. Brain Behav Immun 22:1016–1023.

Thakur M, Crow M, Richards N, Davey GI, Levine E, Kelleher JH, Agley CC, Denk F, Harridge SD, McMahon SB (2014) Defining the nociceptor transcriptome. Front Mol Neurosci 7:87.

Thoreen CC, Chantranupong L, Keys HR, Wang T, Gray NS, Sabatini DM (2012) A unifying model for mTORC1-mediated regulation of mRNA translation. Nature 485:109–113.

Usoskin D, Furlan A, Islam S, Abdo H, Lönnerberg P, Lou D, Hjerling-Leffler J, Haeggström J, Kharchenko O, Kharchenko PV, Linnarsson S, Ernfors P (2015) Unbiased classification of sensory neuron types by large-scale single-cell RNA sequencing. Nat Neurosci 18:145–153.

Uttam S, Wong C, Amorim IS, Jafarnejad SM, Tansley SN, Yang J, Prager-Khoutorsky M, Mogil JS, Gkogkas CG, Khoutorsky A (2018) Translational profiling of dorsal root ganglia and spinal cord in a mouse model of neuropathic pain. Neurobiol Pain 4:35–44.

van den Brink SC, Sage F, Vértesy Á, Spanjaard B, Peterson-Maduro J, Baron CS, Robin C, van Oudenaarden A (2017) Single-cell sequencing reveals dissociation-induced gene expression in tissue subpopulations. Nat Methods 14:935–936.

Wiza C, Nascimento EB, Ouwens DM (2012) Role of PRAS40 in Akt and mTOR signaling in health and disease. Am J Physiol Endocrinol Metab 302:E1453–E1460.

Wolfe AL, Singh K, Zhong Y, Drewe P, Rajasekhar VK, Sanghvi VR, Mavrakis KJ, Jiang M, Roderick JE, Van der Meulen J, Schatz JH, Rodrigo CM, Zhao C, Rondou P, de Stanchina E, Teruya-Feldstein J, Kelliher MA, Speleman F, Porco JA Jr, Pelletier J, et al. (2014) RNA G-quadruplexes cause eIF4A-dependent oncogene translation in cancer. Nature 513:65–70.

Woolf CJ, Ma Q (2007) Nociceptors-noxious stimulus detectors. Neuron 55:353–364.

Xie W, Strong JA, Li H, Zhang JM (2007) Sympathetic sprouting near sensory neurons after nerve injury occurs preferentially on spontaneously active cells and is reduced by early nerve block. J Neurophysiol 97:492–502.

Xie W, Strong JA, Zhang JM (2015) Local knockdown of the NaV1.6 sodium channel reduces pain behaviors, sensory neuron excitability, and sympathetic sprouting in rat models of neuropathic pain. Neuroscience 291:317–330.

Zhou P, Zhang Y, Ma Q, Gu F, Day DS, He A, Zhou B, Li J, Stevens SM, Romo D, Pu WT (2013) Interrogating translational efficiency and lineage-specific transcriptomes using ribosome affinity purification. Proc Natl Acad Sci U S A 110:15395–15400.

Zou D, Silvius D, Fritzsch B, Xu PX (2004) Eya1 and Six1 are essential for early steps of sensory neurogenesis in mammalian cranial placodes. Development 131:5561–5572.